Drillbotics® – Phase I Design Report

International University Competition 2021

Group B (Physical Rig)

Clausthal University of Technology

Institute of Subsurface Technology

Date: December 31st, 2020

Table of Contents

List of Figures and Tables

1 Introduction and Objectives

The 2021 Drillbotics® competition marks the fifth year that a team from the Clausthal University of Technology (TU Clausthal), Germany is participating in the competition. The TU Clausthal opts to participate in the Group B (physical rig) challenge which according to the 2021 Drillbotics® competition guidelines states the objective to "<u>design and build a miniature drilling rig and autonomously drill a directional well through a homogeneous rock sample to a given plan</u>".

Drilling automation is more and more gaining an increased interest from the oil and gas industry, equipment manufactures, and research organizations. Automating the drilling process is considered to offer safety improvements during drilling operations, less drilling time requirements, increasing accuracy in data acquisition, better well placement and quality, and a reduction of costs. In automated drilling systems, the operating parameters are optimized by acquiring relevant data, assessing the data, and adjusting the operating parameters without human interference. Ideally, the automation level reaches tier three, which describes a stage in which the automation has evolved to decide and act autonomously.

The purpose of this proposal is to showcase a well-conceived design plan of a small-scale drilling robot that incorporates important features which are essentially encountered in the field. Emphasis has been placed on implementing different, new ideas and solutions in the design that are not commonly or frequently used in the conventional drilling process to fulfil the demands of directional drilling; utilizing an automated process that from a human intervention point of view only knows the activation of the start button.

This proposal consists of several chapters as follows:

1.   Introduction and Objectives

The *Introduction and Objectives* of this report sets the objectives of the proposal and the project. A brief description of the proposal content is explained herein.

2.   Team and workflow

Team members as well as supervising and advising staff are introduced here. Also, workflow and distribution of workload is described.

3. Rig Design

This chapter explains the rig structure design, the machine bed, the fluid system, the hoisting system, the sled, and the top drive system. The section's dimensions are listed. Further, calculations for pressure loss and cutting transport are presented.

4. Drill Pipe Design

In this chapter the drill pipe characteristics and limit calculations for are presented to determine the maximum values for operating the rig.

5. BHA Design

This chapter explains the bottom hole assembly (BHA) design including the, steering unit, the drill bit and sensor chambers. The developing history leading to the final concept is described. Finally, the chapter includes a brief simulation for the final concept's potential dogleg severity.

6. Mechatronic System Architecture

Within this chapter the mechatronic system, the used sensors, the different actuators and as well the bus system that distributes the operational data will be described. Also, the calibration of the sensors before the drilling operations are discussed.

7. Data Handling

This chapter describes how the acquired sensor dataflow will be processed. Filtration and synchronization of the data as well as the algorithms to use this data for drilling optimization and wellbore trajectory are part of this chapter. Also, the possibility for a third-party interface will shortly be mentioned.

8. Further Rig Considerations

This chapter includes the anticipated total power consumption of the rig, a funding and budgeting plan, a calculation for the rig's shipping weight and a discussion how the rig's design concept could be upscaled.

9. Safety Consideration and Risk Analysis

This chapter discusses the risks and potential harmful events that could occur during the test. Precaution and mitigation plan are set to prevent undesirable events, including the rig structure design and drilling automation system.

This report is an update of the previous design report submitted for the Drillbotics® international university competition 2020.

2 Team and workflow

This year's team of the TU Clausthal's Drillbotics® team will be again working under the supervision of the senior researchers of the drilling and production department of the Institute of Subsurface Energy Systems.

Supervisors:

Dr.-Ing. Javier Holzmann
Dr.-Ing. Carlos A. Paz Carvajal

Two staff members of the drilling and production department of the Institute of Subsurface Energy Systems, who were themselves three times participants in previous Drillbotics® competitions, will serve as advisors to the current team.

Advisors:

Dominik Orgel, M.Sc.
Wolfgang Hollstein, M.Sc.

The competition team of the TU Clausthal consists of five students from different engineering backgrounds.

Student Team:

Felix J.C. Odebrett
Previously attained degree:	B.Sc. in Petroleum Engineering
Current degree:	M.Sc. in Petroleum Engineering major in Drilling and Production
Expected graduation date:	Winter 2021
Role and responsibilities:	Team leader, programming

Dominique F. Briechle
Previously attained degree:	B.Sc. in Petroleum Engineering
Current degree:	M.Sc. in Petroleum Engineering major in Drilling and Production
Expected graduation date:	Summer 2021
Role and responsibilities:	Mechanical design and construction

Felix Krogmann
Previously attained degree:	B.Sc. in Industrial Engineering
Current degree:	M.Sc. in Industrial Engineering major in Production and Processes
Expected graduation date:	Winter 2021
Role and responsibilities:	Programming and algorithm optimization

Rafael Núñez Albermann

Previously attained degree:	B.Sc. in Petroleum Engineering
Current degree:	M.Sc. in Petroleum Engineering major in in Drilling and Production
Expected graduation date:	Summer 2021
Role and responsibilities:	Drilling performance

Marlon Schulz

Previously attained degree:	B.Sc. in Power Systems Technologies
Current degree:	M.Sc. in Power Systems Engineering major in Renewable Power Engineering
Expected graduation date:	Summer 2022
Role and responsibilities:	Electrical engineering

Previous participations in the Drillbotics® competition from the TU Clausthal showed that distinct distribution of workload and clear communication between the team members is crucial for success. That realization lead to the conclusion to distribute the different tasks involved in designing and building the autonomous drilling rig from the very beginning between the different team members. One team member purely focuses on the mechanical design of the different rig and BHA parts while another team member concentrates on the electronic parts like sensors, actuators, and circuit boards. Two team members are exclusively working on the programming and implementing of the data handling and control algorithms. The team leader serves as a connector between the different team members and must ensure that the overall concept is followed. He distributes the different tasks and keeps track of the progress. Weekly meetings of the whole team and the two advisors are held to exchange new developments and to get everybody on the same level of knowledge. Further working meetings in smaller groups are taking place regularly as well. All produced files and information are saved in a cloud computing environment, to which all team members have access. An overview of the tasks that are completed, in progress or planned are displayed in a workflow accessible for all team members. Due to the ongoing restrictions in Germany caused by the efforts to fight the current worldwide pandemic, most team members work from home and meetings are held online. Access to the mechanical rig in the institute's building is only granted for single students under hygienic precautions. Due to these special circumstances, a good communication and coordination between the team members is essential.

3 Rig Design

3.1 Rig Overview

For the 2021 competition a new design is proposed to accommodate the rotary BHA system. The new rig, as illustrated in **Figure 1.**, will consist mainly of a traverse which can be disconnected from the main construction. The traverse is mounted on four pivots and supports drilling in any pre-defined position, i.e. in vertical or horizontal starting position. A higher grade of transportability is achieved with this specific design choice. A surface power pack is used to rotate a flexible shaft which is coated from the drill pipe. The bottom part of the shaft is connected to the bit. This design allows to rotate the bit via the flexible shaft without rotating the drill pipe. As a push-the-bit system is used (see **Chapter 5**), rotation of the drill pipe needs to be prevented. The overall size of the rig and its components are displayed in **Table 1**.
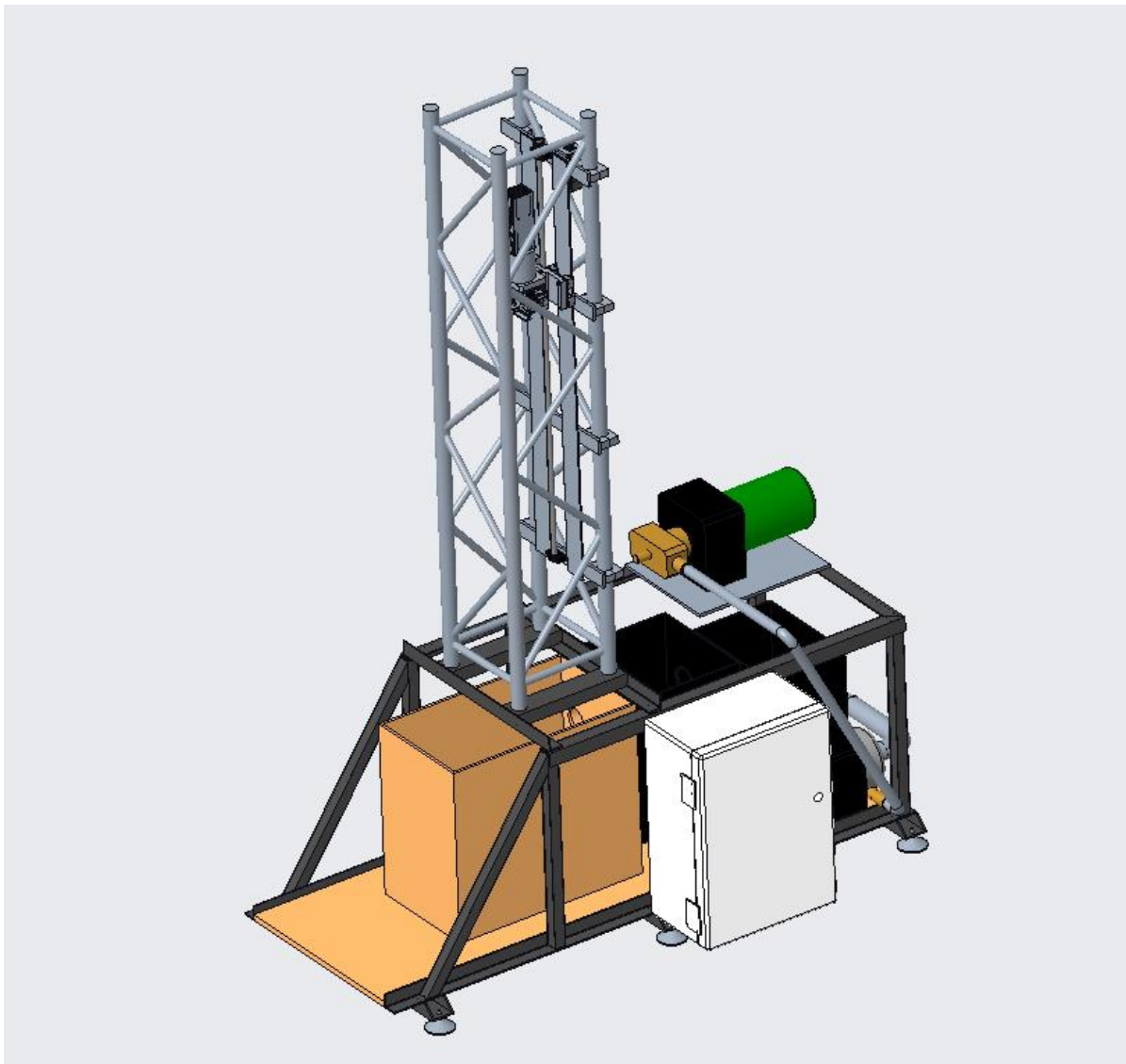
Figure 1: Rig overview

Table 1: **Rig components' dimensions**

Component	Height (cm)	Length (cm)	Width (cm)	Volume (L)
Rock sample receiver	60	68	38	155
Mounting System	80	200	79	-
Traverse System	200	40	40	-
Topdrive	28	9,5	9,5	-
Syringe System	15	14	20	-
BHA	15,4	3,3	3,3	-

3.2 Rotary Table and Power Pack

To be able to point the drill bit into any desired spherical coordinate, the BHA must be rotated in the desired direction. To achieve this, a rotary table has been incorporated into the design of the rig. A form-locked and friction locked connection to the drill string by means of a collet chuck assembly is applied and, thus, can position the drill string to achieve a precise angle. Azimuth corrections are also enabled by steering the drill string.

In contrast to the concept of last year, this year's construction features a rotary table mounted driving motor. As driving motor, this year a Teknomotor C31-40 as shown in **Figure 2** was chosen, which has enough power and rpm to propel the used flex shaft in order to provide downhole torque and speed. As the flexible shaft runs within the drill pipe, cables and hoses cannot be accommodated within the pipe. The data and power supply cables as well as the hoses for drilling mud and hydraulic fluids are therefore attached outside to the drill pipe. A rotary decoupler is attached to the motor allowing the hoses and cables to rotate with the rotary table and hence the drill pipe.

3.3 Rock Sample Receiver

The rock sample receiver (**Figure 3**) of this year's rig is a simple quadratic box, as illustrated in the image beneath the section, where the rock sample will be hoisted in. The sampling receiver is connected to the mud filtration to separate the drilling fluid into its different components. In contrast to last year's installation, this year's receiver will feature a mounted beam on top with a centralizer tube in order to stabilize the BHA before it enters the rock sample completely.

Figure 2: **Rotary Table and Teknomotor**
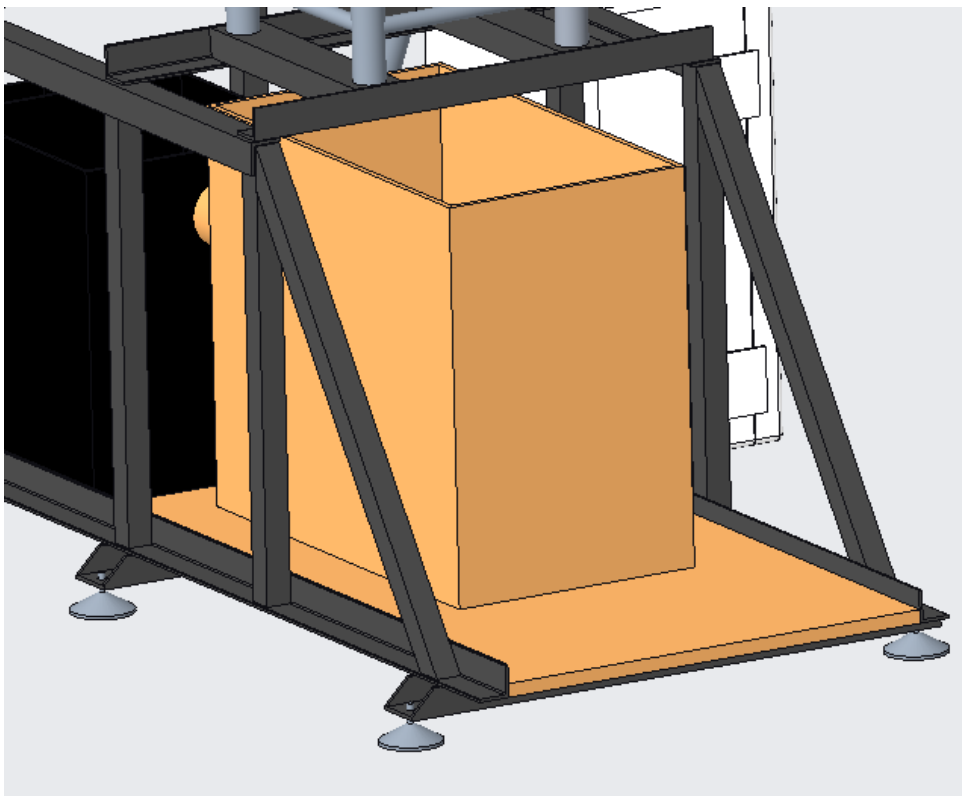
Figure 3: **Rock sample receiver**

3.4 Rig Electronics

The electronics are housed in a switch cabinet under the rig table and protected against water. In addition, FI circuit breakers are installed to interrupt the power supply immediately in the event of a failure.

The main computer with the human machine interface will be located on the table next to the main controller. Thus, the current state during drilling can be easily tracked and monitored.

3.5 Rig Plumbing and Mud Handling

A drilling mud preparation container is installed next to the drilling sample container. Behind the filter, a pump is connected which generates the necessary pump pressure for drilling. The pumps used for the setup are a combination of a pre charging pump (2-3 bar pre-pressure), that feed a positive displacement pump with a maximum pressure capacity of 120 bar.

The drilling mud will be pumped through a plastic hose that is connected outside to the drill pipe. The hose will lead into the BHA and the drilling mud is then directed to the bit and leaves the bit through its nozzles. The returning drilling mud will be handled by a two-chambered separation tank system. The drilling mud will be drawn out of the rock sampling receiver and will be floated into the first mud tank. In there, the heavier components will be separated due to the gravitational force and only the liquid components will enter the next tank. Due to the slow flow rate of the systems fluid, there is enough time to separate the solid from the liquid components of the mud. The last tank will be connected to a pumping system to reinject the filtered drilling mud into the hose. Inside the mud tanks, filtration packs consisting of plastic granules are installed to increase filtration performance of the mud handling system. Water with no additives will be used as drilling mud. Any other decision would lead to higher environmental impacts and to the need to a very thorough and complex sealing and leakage prevention. Also, the need for additives or an oil-based mud is not seen for the given application.

Basis for the circulation system were the cutting transport and pressure loss calculations which are presented in the following two sub-chapters. The used values can be found in **Appendix B**.

3.5.1 Cutting Transport Calculation

The following section sets the flow rate calculation required for drilling operation, for a Newtonian fluid. The minimum flow rate of the mud v_{mud} must be greater than the terminal slip velocity v_{SliTer} expressed in following equation:

$$v_{mud} > v_{SliTer} \qquad (1)$$

The slip velocity can be calculated by Moore's correlation for a vertical well.

The slip velocity of a small spherical particle settling (slipping) through a Newtonian fluid under laminar flow condition, v_{slips} is given by Stoke's law:

$$v_{slip} = \frac{138 * (\rho_s - \rho_f) * d_s^2}{\mu_a} = \frac{138 * (22.07 - 8.33) * 0.004^2}{1}$$

$$= 0.0303 \frac{ft}{s} \quad \left(0.0092 \frac{m}{s}\right) \qquad (2)$$

Where:

d_s: Diameter of cutting

ρ_s: Density of the cutting solid

ρ_f: Density of the drilling fluid (density of water)

μ_a: Viscosity of the drilling fluid (viscosity of water)

After determining the Particle Reynolds number Re_p:

$$Re_p = \frac{928 * \rho_f * v_{slips} * d_s}{\mu_a} = \frac{928 * 8.33 * 0.0303 * 0.004}{1} = 0.936 \qquad (3)$$

where:

ρ_f: Density of the drilling fluid (density of water)

d_s: Diameter of cutting

μ_a: Viscosity of the drilling fluid (viscosity of water)

v_{slips}: Slip velocity from previous calculation

the friction factor f is taken as 42.7 according to Moore's correlation, then the terminal slip velocity, v_{SliTer}, is calculated again:

$$v_{SliTer} = f * \sqrt{d_s \frac{(\rho_s - \rho_f)}{\rho_f}} = 42.7 * \sqrt{0.004 * \frac{(22.07 - 8.33)}{8.33}}$$

$$= 3.47 \frac{ft}{s} \quad \left(1.06 \frac{m}{s}\right) \qquad (4)$$

Where:

ρ_s: Density of the cutting solid

ρ_f: Density of the drilling fluid (density of water)

d_s: Diameter of cutting

Slip velocity Stokes law

$$Re = \frac{928 * \rho_f * v_{slips} * d_s}{\mu_a}$$

$Re < 3$

$$f = \frac{40}{Re}$$

$3 < Re < 300$

$$f = \frac{22}{\sqrt{Re}}$$

$Re > 300$

$f = 1.54$

$$v_{slip} = f * \sqrt{d_s \frac{(\rho_s - \rho_f)}{\rho_f}}$$

$$abs\left|v_{slip} - v_{slips}\right| < 0.001$$

$$v_{slip} = \frac{v_{slip} - v_{slips}}{2}$$

v_{slip} = slip velocity Moore
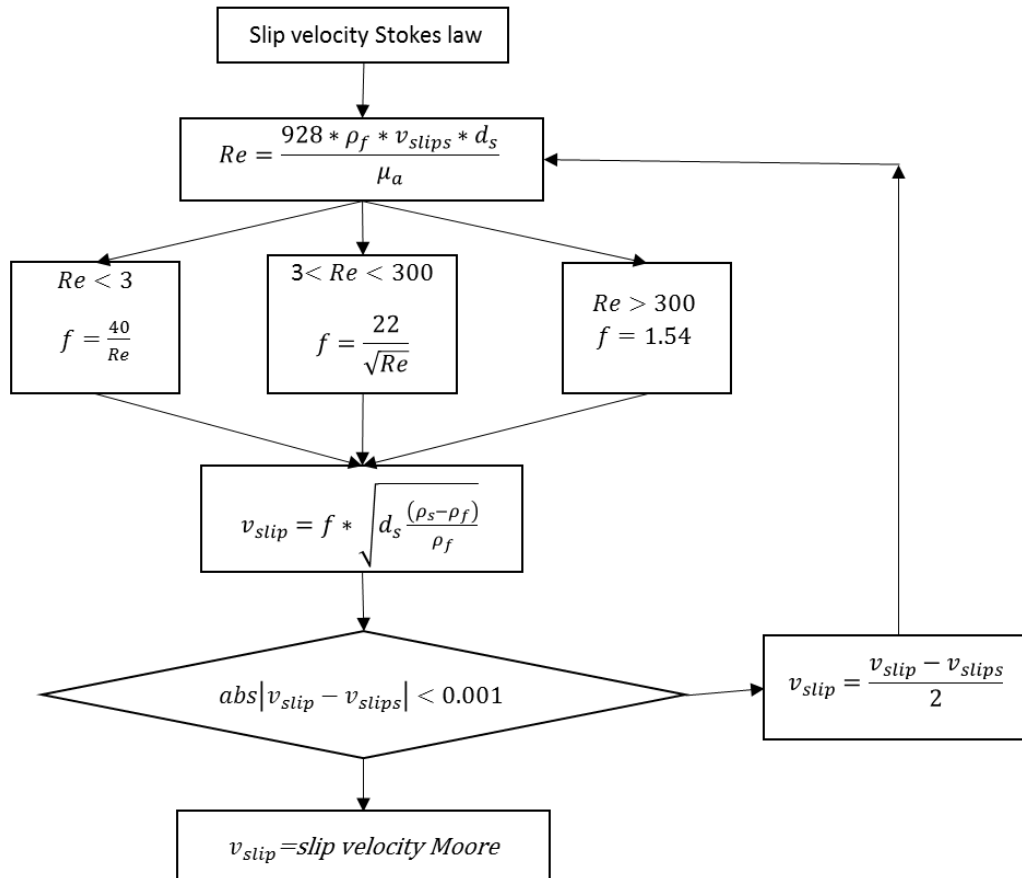
Figure 4: **Slip velocity derived by Moore's correlation**

Therefore, the mud velocity must be at least as high as 3.47 ft/s.

A flow rate of 1.85 gpm (7 L/min) is pumped by the rig pump. The annular velocity v_a is calculated by following formula:

$$v_a = \frac{Q}{2.448 * (d_h^2 - d_d^2)} = \frac{1.85}{2.448 * (1.5^2 - 1.46^2)} = 6.38 \frac{ft}{s} \quad \left(1.94 \frac{m}{s}\right) \quad (5)$$

Where:

Q: Flow rate of drilling fluid

d_h: Borehole diameter

d_d: Outside diameter of the downhole stabilizer

For the transport ratio a value of above 50% is empirically recommended to achieve good hole-cleaning during drilling. The transport ratio is calculated as follows and a value of 88 % determined:

$$Transport\ ratio = \frac{v_a - v_{mud}}{v_a} * 100 = \frac{6.38 - 3.47}{6.38} * 100 = 45.6\% \qquad (6)$$

Where:

v_a: Annular velocity of drilling fluid

v_{mud}: Mud velocity

3.5.2 Pressure Loss Calculation

The following section sets the calculation for conventional, rotary drilling pump requirements with the bit dimensions provided by DSATS. Assuming the Newtonian fluid (water) flow inside the hose around the drill string, the pressure loss inside the hose along the drill pipe is calculated as follows.

First the velocity of the fluid in the hose v_d is determined:

$$v_d = \frac{Q}{2.448 * (id_p^2)} = \frac{1.84}{2.448 * (0.275^2)} = 9.94 \frac{ft}{s} \quad \left(3.03 \frac{m}{s}\right) \qquad (7)$$

Where:

Q: Flow rate of drilling fluid

id_p: Internal diameter of the drill pipe

Based on that, the Reynolds number is determined:

$$Re = \frac{928 * \rho_f * v_d * id_p}{\mu_a} = \frac{928 * 8.33 * 9.94 * 0.275}{1} = 21188\ (Turbulent) \qquad (8)$$

Where:

ρ_f: Density of the drilling fluid (density of water)

v_d: Velocity of the drilling fluid inside the drill pipe

id_p: Internal diameter of the drill pipe

μ_a: Viscosity of the drilling fluid (viscosity of water)

The required friction factor f can be calculated by the following formula:

$$f = 0.25 \left[log_{10} \left(\frac{\in}{3.7 * id_p} + \frac{5.74}{Re^{0.9}} \right) \right]^{-2} = 0.25 \left[log_{10} \left(\frac{0.0006}{3.7 * 0.275} + \frac{5.74}{21188^{0.9}} \right) \right]^{-2}$$
$$= 0.0301 \qquad \textbf{(9)}$$

Where:

$\in$:   Roughness of the drill pipe (assumed with 0.0006 in)

id_p: Internal diameter of the drill pipe

Re: Reynolds number

The pressure loss inside the drill pipe, P_s, is calculated as follows:

$$P_s = \frac{f * \rho_f * v_d^2 * L_{string}}{25.8 * id_p} = \frac{0.0301 * 8.33 * 9.94^2 * 3}{25.8 * 0.275} = 10.48 \, psi \quad (0.72 \, bar) \qquad \textbf{(10)}$$

Where:

f: Fanning friction factor

v_d: Velocity of the drilling fluid inside the drill pipe

L_{string}: Length of the drillstring

id_p: Internal diameter of the drill pipe

p_f: Viscosity of the drilling fluid (water)

In addition, the pressure loss within the BHA must be calculated. It is the sum of the pressure losses in the flow line parallel to the first shaft and the losses within the rotating hollow shaft:

First the Losses inside the flow line are calculated.

Fluid velocity:

$$v_{fl} = \frac{Q}{2.448 * \left(id_{fl}^2 \right)} = \frac{1.84}{2.448 * (0.157^2)} = 30.45 \frac{ft}{s} \quad \left(9.29 \frac{m}{s} \right) \qquad \textbf{(11)}$$

Where:

v_{fl}:   Velocity of the drilling fluid inside the flow line

Q: Flow Rate

id_{fl}:   Internal diameter of the flow line

Reynolds Number:

$$Re = \frac{928 * \rho_f * v_{fl} * id_{fl}}{\mu_a} = \frac{928 * 8.33 * 30.45 * 0.157}{1} = 37080 \ (Turbulent) \qquad (12)$$

Where:

Re: Reynolds Number

ρ_f: Drilling fluid density

v_{fl}:   Velocity of the drilling fluid inside the flow line

id_{fl}:   Internal diameter of the flow line

μ_a: Viscosity of the drilling fluid (viscosity of water)

Friction factor:

$$f = 0.25 \left[log_{10} \left(\frac{\in}{3.7 * id_{fl}} + \frac{5.74}{Re^{0.9}} \right) \right]^{-2} = 0.25 \left[log_{10} \left(\frac{0.0039}{3.7 * 0.157} + \frac{5.74}{37080^{0.9}} \right) \right]^{-2}$$
$$= 0.0544 \qquad (13)$$

Where:

$\in$:   Roughness of the flow line (0.0039 in)

id_{fl}:   Internal diameter of the flow line

Re: Reynolds Number

Pressure Losses:

$$P_{fl} = \frac{f * \rho_f * v_{fl}^2 * L_{fl}}{25.8 * id_{fl}} = \frac{0.0544 * 8.33 * 30.45^2 * 0.4}{25.8 * 0.157} = 42.13 \ psi \quad (2.9 \ bar) \qquad (14)$$

Where:

f: Fanning friction factor

ρ_f: Density of drilling fluid

L_{fl}:   Length of flow line

v_{fl}:   Velocity of the drilling fluid inside the flow line

id_{fl}:   Internal diameter of the flow line

Second the Losses inside the hollow shaft are calculated.

Fluid velocity:

$$v_{sh} = \frac{Q}{2.448 * (id_{sh}^2)} = \frac{1.84}{2.448 * (0.196^2)} = 19.49 \frac{ft}{s} \quad \left(5.94 \frac{m}{s}\right) \qquad (15)$$

Where:

v_{sh}: Velocity of the drilling fluid inside the shaft

Q: Flow Rate

id_{sh}: Internal diameter of the shaft

Reynolds Number:

$$Re = \frac{928 * \rho_f * v_{sh} * id_{sh}}{\mu_a} = \frac{928 * 8.33 * 19.49 * 0.196}{1} = 29664 \ (Turbulent) \qquad (16)$$

Where:

Re: Reynolds Number

ρ_f: Drilling fluid density

v_{sh}: Velocity of the drilling fluid inside the shaft

id_{sh}: Internal diameter of the shaft

μ_a: Viscosity of the drilling fluid (viscosity of water)

Friction factor:

$$f = 0.25 \left[log_{10} \left(\frac{\epsilon}{3.7 * id_{sh}} + \frac{5.74}{Re^{0.9}} \right) \right]^{-2} = 0.25 \left[log_{10} \left(\frac{0.0039}{3.7 * 0.196} + \frac{5.74}{29664^{0.9}} \right) \right]^{-2}$$
$$= 0.0504 \qquad (17)$$

Where:

ϵ: Roughness of the flow line (0.0039 in)

id_{sh}: Internal diameter of the shaft

Re: Reynolds Number

Pressure Losses:

$$P_{sh} = \frac{f * \rho_f * v_{sh}^2 * L_{sh}}{25.8 * id_{sh}} = \frac{0.0504 * 8.33 * 19.49^2 * 0.19}{25.8 * 0.196} = 6.19 \, psi \quad (0.42 \, bar) \quad \textbf{(18)}$$

Where:

f: Fanning friction factor

ρ_f: Density of drilling fluid

L_{sh}: Length of the shaft

v_{sh}: Velocity of the drilling fluid inside the shaft

id_{sh}: Internal diameter of the shaft

Finally, the previously calculated losses are summed up to acquire the BHA pressure losses:

$$6.19 + 42.13 = 48.33 \, psi \quad (3.33 \, bar) \quad \textbf{(19)}$$

Where:

P_{sh}: Pressure losses in the shaft

P_{fl}: Pressure losses in the flow line

There are three nozzles at the bit. For that reason, the total area of nozzle, A_n, is calculated as follows:

$$A_n = 3 * \frac{\pi}{4} * d_n^2 = 3 * \frac{\pi}{4} * 0.118^2 = 0.008 in^2 \quad (0.053 cm^2) \quad \textbf{(20)}$$

Where:

d_n: Nozzle diameter

Then, the pressure loss at the bit, P_{bit} can be estimated by following calculation:

$$P_{bit} = \frac{Q^2 * \rho_f}{12031 * A_n^2} = \frac{1.84^2 * 8.33}{12031 * 0.008^2} = 35.06 \, psi \quad (2.41 \, bar) \quad \textbf{(21)}$$

The jet impact force, F_j of the bit is:

$$F_j = 0.01823 * C_d * Q * \sqrt{\rho_f P_{bit}} = 0.01823 * 0.95 * 3.51 * \sqrt{8.33 * 126.3}$$
$$= 0.54 \; lbf \quad (2.43 \; N) \quad (\mathbf{22})$$

Where:

C_d: Discharge coefficient (assumed value ~ 95%)

Q: Flow rate of drilling fluid

ρ_f: Density of the drilling fluid (density of water)

P_{bit}:   Pressure loss at the bit

The jet velocity of the bit, v_{bit} is:

$$v_{bit} = \frac{Q}{A_n} = \frac{1.84 * 144}{7.48 * 60 * 0.008} = 73.79 \frac{ft}{s} \quad \left(22.5 \frac{m}{s}\right) \quad (\mathbf{23})$$

Where:

Q: Flow rate of drilling fluid

A_n: Total area of the nozzles

Further, the pressure loss in annulus, P_a is calculated as follows:

$$P_a = \frac{1.4327 * 10^{-7} * \rho_f * L_{rock} * v_a^2}{(d_h - d_d)} = \frac{1.4327 * 10^{-7} * 8.33 * 2 * 1.97 * 153.1^2}{(1.5 - 1.45)}$$

$$= 6.8 \; psi \quad (0.46 \; bar) \quad (\mathbf{24})$$

Where,

ρ_f: Density of the drilling fluid (density of water)

L_{rock}:   Length of the rock sample

v_a: Annular velocity of the drilling fluid

d_h: Borehole diameter

d_d: Outside diameter of the downhole stabilizer

The annular velocity is 353.9 ft/min (107.8 m/min). The total downhole pressure loss, $P_{downhole}$ is the sum of the following:

$$P_{downhole} = P_s + P_{bit} + P_a + P_{BHA} = 10.48 + 35.06 + 6.8 + 48.33$$
$$= 100.68 \, psi \quad (6.94 \, bar) \quad (\mathbf{25})$$

It is assumed that the pump will be connected with the hose line (made from rubber material) to the standpipe with roughness 0.0006 in. The pressure loss in the hose, P_h is calculated by following the same schematic as applied for the pressure loss calculation before:

$$v_h = \frac{Q}{2.448 * (id_h^2)} = \frac{1.84}{2.448 * (0.5^2)} = 3.02 \frac{ft}{s} \quad \left(0.92 \frac{m}{s}\right) \quad (\mathbf{26})$$

$$Re = \frac{928 * \rho_f * v_h * id_h}{\mu_a} = \frac{928 * 8.33 * 3.02 * 0.5}{1} = 11678 \, (Turbulent) \quad (\mathbf{27})$$

Where:

Q: Flow rate of drilling fluid

id_h: Internal diameter of the rubber hose

ρ_f: Density of the drilling fluid (density of water)

v_h: Velocity of the drilling fluid inside the hose

Then, the ratio of the roughness of the pipe divided by the inner diameter of the pipe $\in/id_p$ is calculated to determine the friction factor on the Fanning chart, as shown in **Figure 5**:

$$\frac{\in}{id_h} = \frac{0.0006}{0.5} = 0.0012 \quad (\mathbf{28})$$

Where:

$\in$:   Roughness of the rubber hose

id_h: Internal diameter of the rubber hose
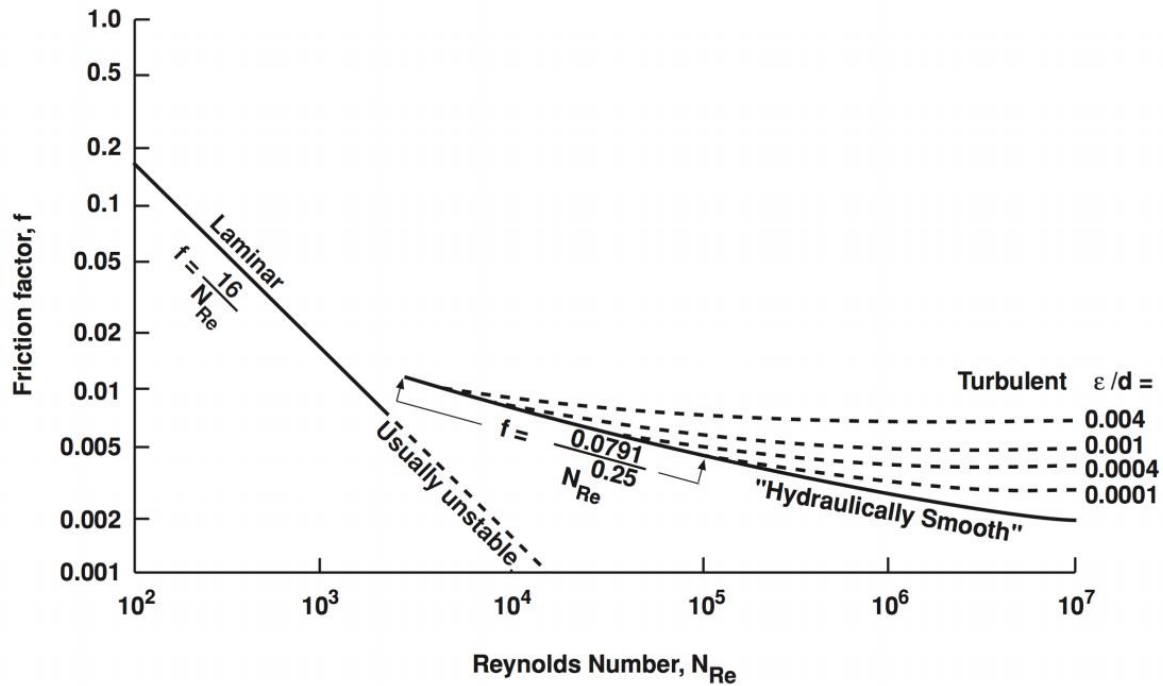
Figure 5: Fanning chart; friction factors for turbulent flow in circular pipes

Based on the Fanning chart, see Figure 4, the friction factor, f, is approximately 0.007. The pressure loss inside the hose, P_h is:

$$P_h = \frac{f * \rho_f * v_h^2 * H_{rig}}{25.8 * id_h} = \frac{0.007 * 8.33 * 3.02^2 * 7.5}{25.8 * 0.5} = 0.3 \, psi \quad (0.02 \, bar) \quad \textbf{(29)}$$

Where:

f: Fanning friction factor

v_h: Annular velocity of the drilling fluid inside rubber hose

H_{rig}:   The height of the rig

id_h: Internal diameter of the rubber hose

The total pressure loss along the entire system is:

$$Total\ pressure\ loss = P_{downhole} + P_h = 100.99 \, psi \quad (6.96 \, bar) \quad \textbf{(30)}$$

Where:

P_h: Pressure loss inside rubber hose

The total pressure loss with additional atmospheric pressure is 349.05 psi (24.07 bar). To estimate the pump horsepower requirement, Bernoulli's equation is used:

$$P_{pump} = P_{loss} + P_{atm} + \frac{\rho_f * \Delta v^2}{2} + \rho_f * g * \Delta h$$

$$= 100.99 + 14.5 + \frac{8.33 * 7.48 * (3.02^2 - 5.89^2)}{2 * 32.174 * 144} + \frac{8.33 * 7.48 * 32.174 * (7.5)}{32.174 * 144}$$

$$= 118.76 \, psi \quad (8.19 \, bar) \quad \textbf{(31)}$$

$$Pump_{HP} = \frac{P*Q}{1714} = \frac{118.76*1.84}{1714} = 0.12 \, HP \quad (0.09 \, kW) \quad \textbf{(32)}$$

Where:

P_{loss}: Pressure loss inside the circulation system

P_{atm}: Atmospheric pressure

ρ_f: Density of the drilling fluid (density of water)

Δh: The height of the rig, H_{rig}

g: Earth gravitation, 32.174 ft/s²

P: Total pressure required

Q: Flow rate of drilling fluid

Conversion from ft³ to gallon: 7.48

Conversion from ft² to in²: 144

It is assumed that the efficiency of the pump is 85%, therefore the requirement of the horsepower pump is 0.12 HP (0.09 kW). The following **Table 2** shows the variation of the pump power requirement according to the flow rate variation:

Table 2: **Pump power requirement rotary drilling**

Flow rate variation (gpm)	Flow rate variation (Lpm)	Transport ratio (%)	Pump Pressure (bar)	Pump (HP)	Pump (kW)
1.32	5	70	4.82	0.05	0,04
1.84	7	83	8.19	0,12	0,09
2.64	10	85	15.3	0.34	0,25
3.43	13	88	24.89	0.72	0.53

4 Drill Pipe

The original rig featured an aluminium drill pipe. Since last year, the guidelines allow for a steel drill pipe to be used for the rig. Due to the higher stability and durability, it was decided to upgrade the rig with a steel pipe. The diameters, the density and Young's modulus of the selected pipe can be found in **Appendix B**. The 0.91 m long pipe is constructed in one piece and hence does not need tool joints. The pipe is connected with the top drive and the BHA with collect chuck joints. Through the pipe runs the before mentioned flexible shaft. Based on the selected pipe; the following limit calculations were conducted. The flexibility of the pipe and its impact on directional drilling will be discussed in **Chapter 5.2.6**

4.1 Limit Calculations

The steel drill pipe can be considered as one of the weakest parts in the entire string next to a connection. The following calculated values for buckling, burst and torsion maxima, are based on the scenario that no other forces are acting on the component for the calculation. The maximum values are good indicators, aiding in the selection of the appropriate equipment and parameters for the drilling robot, such as the maximum WOB for the hoisting system, maximum torque value for the Downhole motor, and high pump pressures for flushing. The used values can be found in **Appendix B**.

4.2 Buckling Limit Calculation

Buckling is characterized by a lateral deformation or failure of a structural member subjected to high axial compressive stress, where the compressive stress at the point of failure is less than the yield strength that the material can withstand. The critical buckling load limit of the steel drill pipe is calculated by the following Euler equation (assuming both pipe ends are pinned). First the moment of inertia I is determined:

$$I = \frac{\pi}{64}\left(d_p^4 - id_p^4\right) = \frac{\pi}{64}\left(0.393^4 - 0.315^4\right)$$
$$= 6.876 * 10^{-4} in^4 \quad (2.862 * 10^{-10} m^4) \quad \textbf{(33)}$$

Where:

d_p: Outside diameter of the drill pipe

id_p: Inside diameter of the drill pipe

Then the critical buckling load,P_{cr}, is calculated:

$$P_{bcr} = \frac{\pi^2 * E * I}{(K * L)^2} = \frac{\pi^2 * 2.901 * 10^7 * 6.8790 * 10^{-4}}{(1 * 36)^2})$$

$$= 151.92 \; lbf \quad (75.77 \; N \; or \; 68.91 \; kg \qquad (\mathbf{34})$$

Where:

P_{bcr}: Critical buckling load

E: Modulus elasticity of the steel drill pipe

I: Area moment of inertia

L: Length of the column

K: Column effective length factor

Based on the scenarios of buckling failure, there are several recommendations in respect to the effective length factor (K), as illustrated in **Figure 6.** and **Table 3**. The variation of effective length factor is used to estimate the buckling load limit.

Buckled shape of column shown by dashed line						
Theoretical K value	0.5	0.7	1.0	1.0	2.0	2.0
Recommended design value K	0.65	0.80	1.2	1.0	2.10	2.0
End condition key		Rotation fixed and translation fixed				
		Rotation free and translation fixed				
		Rotation fixed and translation free				
		Rotation free and translation free				

Figure 6: **Design value K variation**

Table 3: Buckling limit according to K variation

K variation	Buckling load limit (lbf)	Buckling load limit (N)	Buckling load limit (Kg)
0.5	607.67	2703.05	275.63
0.7	310.04	1379.13	140.63
1	151.92	675.77	68.91
2	37.98	168.94	17.22

4.3 Burst Limit Calculation

Assuming the yield strength, of the steel drill pipe is 31183 psi (215 MPa) and a safety factor 1.5, the burst limit, P_{burst}, of the steel drill pipe can be estimated by following equation (Barlow equation):

$$P_{burst} = \frac{2 * Y_p * t}{d_p * Sf} = \frac{2 * 31183 * 0.0787}{0.393 * 1.5} = 8326.04 \ psi \quad (574.06 \ bar) \quad (35)$$

Where,

Y_p: Yield strength of the drill pipe

t: Wall thickness of the drill pipe

d_p: Outside diameter of the drill pipe

Sf: Safety factor

4.4 Torsional Limit Calculation

Assuming the maximum yield stress of the steel drill pipe is 31183 psi (215 MPa), the maximum limit of torque T_{max} of the steel drill pipe can be estimated by following equation:

$$T_{max} = \frac{\pi}{16} * \sigma_{max} * \frac{\left(d_p^4 - id_p^4\right)}{d_p} = \frac{\pi}{16} * 31183 * \frac{(0.393^4 - 0.315^4)}{0.393}$$

$$= 218.25 \ in.lbf \quad (24.66 \ Nm) \quad (36)$$

Where,

d_p: Outside diameter of the drill pipe

id_p: Inside diameter of the drill pipe

σ_{max}:   Yield strength of the drill pipe

5 BHA Design

Due to the usage of a 1.5 Inch diameter Bit the 2019 Drillbotics® Competition, the TU Clausthal chose once more a larger diameter for their drill bit and BHA construction. This year´s concept is based around a drill bit propelled by a flexible shaft, which is powered by a surface mounted electric motor used normally for milling applications. The BHA is steerable through three independent wings following a push-the-bit approach and allows an inclination setup of 9 degrees.

5.1 Development History

Different approaches were discussed in the team taking many considerations into account. Until the final concept was decided on, earlier ideas were favoured. For the sake of completeness and to better understand the development history, the earlier concepts are described as follows.

5.1.1 Concept 1

The first concept (**Figure 7**) was based around a BLDC Downhole Motor and a radial bending joint, which allowed the setting of a specific inclination towards the central axis. This concept study resulted in a very long BHA setup and therefore it would have been difficult to meet the drilling requirements of the given trajectory. Furthermore, the stresses along the outer borehole wall could have led to a total failure of the construction due to the high axial forces alongside the BHA during the bending process.
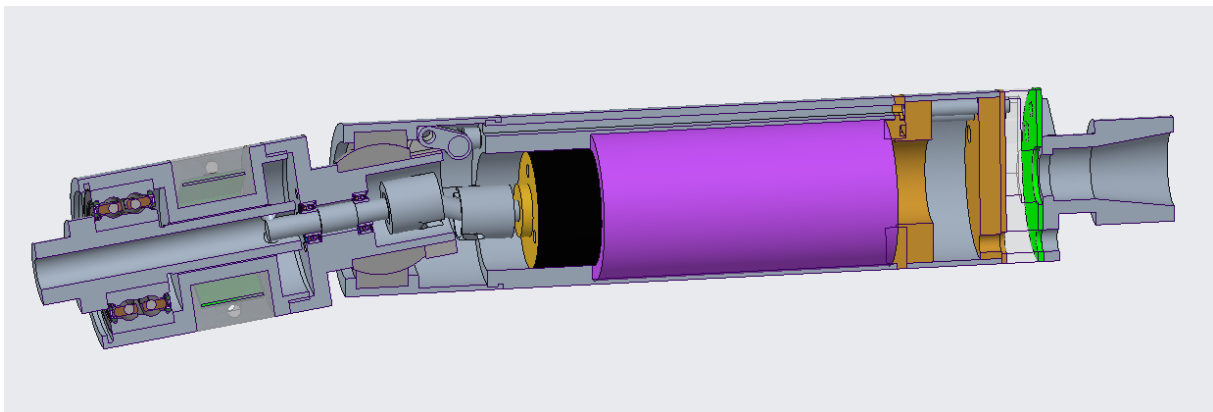
Figure 7: **Bendable BHA construction**

5.1.2 Concept 2

The second concept was as well based around a BLDC Motor but instead of a radial bending joint the steering requirements would have been meet with the help of two extendable wings (**Figure 8**), which allowed a correction of inclination towards the borehole wall. The wings could be steered independent

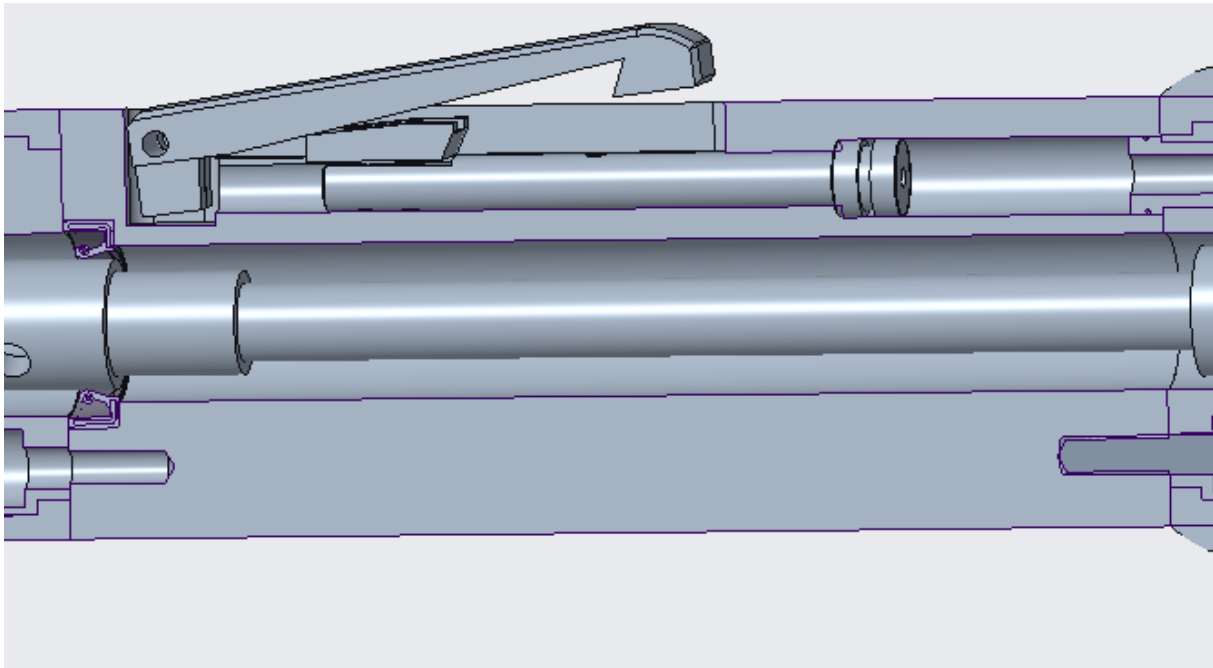from one another with two hydraulic cylinders. The extended wings would have been pressed against the borehole wall and by that would have ensured, that the inclination correction is carried out.

Figure 8: **Wing Module extended**

5.1.3 Concept 3

Finally, it was decided to change the concept drastically due to the limited space of the BHA. The driving Motor is now installed onto the rotary table and is powering the bit with the help of a flex shaft. The concept of the rest of the bottom hole assembly however remained the same as in the second development stage. An optional setup consists of three wings instead of two in order to increase stability of the BHA during the drilling operation.

5.2 Description of the Final Concept

This year's BHA consist of a modular system, which allows the team to adjust the system to the different wellbore conditions. The upper part of the system consists of a modular guiding plate setup, which manages the incoming fluids from the surface. The fluids are directed to their specific destination with this modular channeling system. In total the setup consists of five different input ports, three of them for the high-pressure cables, one for the drilling fluid and the last one for the electrical cables.

5.2.1 Collet Chuck Joint

A notch will be considered to hold a sensor unit in the upper unit. In the same way, this type of notch is also placed directly behind the bearing package in the

lower unit. Between drill string and collet chuck receiver, there are two O-rings to prevent water from breaking into the electronics compartment. The collet chuck is tightened by a union nut. With this type of clamping, the cross section of the drill string is not disturbed, and more force can be transmitted.

5.2.2 Safety Clutch

Since the flex shaft can only transmit a maximum torque of 6 Nm before permanent damage is imminent, a way had to be found to prevent failure. This can happen if the drill bit seizes up and the energy stored in the inertia is suddenly transferred to the flex shaft in the form of excessive torque. In order to avoid such a scenario in operation, it was decided to use a clutch which rotatably separates the flex shaft from the drill bit when the torque exceeds a certain level, so that damage to the shaft, which is difficult to replace, is avoided. The clutch (**Figure 9**) is designed in such a way that three balls under spring pre-tension engage in bores which are located radially in the clutch bell and thus the torque is transmitted via the shear forces. If the transmitting torque increases in a forcible manner, the balls slip out of the slightly smaller bore holes and the clutch allows the Flex shaft to rotate freely. In order to achieve the best possible performance in later operation, an adjusting screw has been designed to adjust the preload of the spring. In this way an optimum can be determined experimentally. In addition, the speed of the main shaft is determined by the sensor module and the algorithm recognizes the triggering of the clutch and thus also a seizing of the bit, so that countermeasures can be taken. Due to its complex design, it is still under discussion if the safety clutch will be implemented or if a workaround can be found.
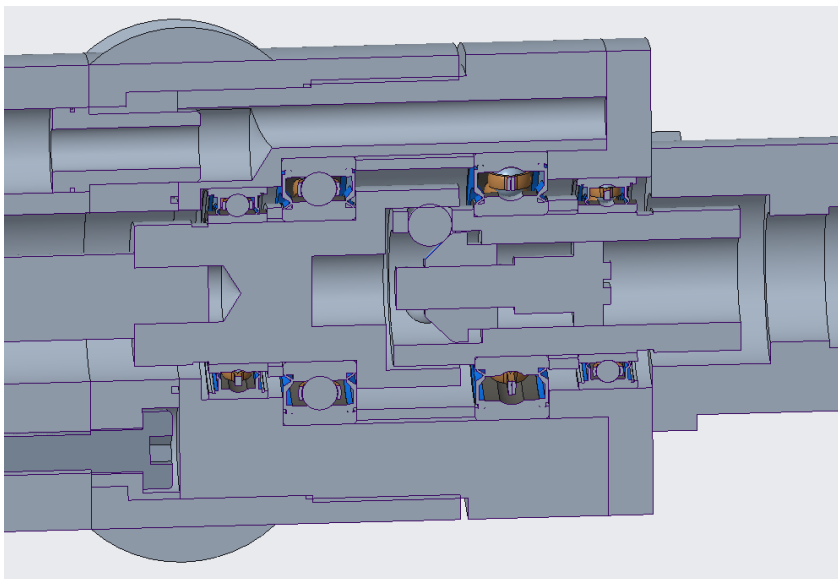
Figure 9: **Prevention Clutch**

5.2.3 Stabilizer

The stabilizer of the Bottom Hole Assembly is attached to the prevention clutch and is responsible for the overall borehole quality. The stabilizer centers the BHA inside the hole and therefore prevents shifting of the BHA during the drilling operation and establishes the fixation of the BHA during downhole operations. The stabilizing element consist of seven convex shaped fins, that can guide the BHA along the drill path. Further, it can reduce the shocks transmitted through the pipe and the rotating shaft onto the BHA and therefore prevents the bit from lateral displacement due to vibrations.

5.2.4 Steering Unit

The steering unit is connected underneath the upper safety clutch part. This year´s steerable component consists of two or three wings, that can be extended due to the inflow of liquid under high pressure conditions into three independent cylinders. Each wing is independently controllable from one another and can be unfolded by its own cylinder steering unit. The cylinders are attached to a wedge which will drive the wings from its current position. To reduce the current inclination, three springs, one for each cylinder, are included in the construction to reposition the lifting arms of the cylinders. The inflow of the high pressurized liquid into the cylinders will be managed through surface mounted stepper motors, which will allow to control inflow and outflow without the hazard of pumping a vacuum.

5.2.5 Syringe Unit

The subsurface steering unit is powered by a surface mounted control device (**Figure 10**), allowing the wings to be actuated separately throughout a cable system and a fluid injection system. The whole subsurface compartment is stored on top of the topdrive and will function through actuated stepper motors, that are connected to the processing unit to adjust the total deflection of the bottom hole setup. The pressure is recorded by a sensor for each of the three cables, that enables the processing unit to extrapolate the grade of deflection of the drill curve. If the deflection in one direction should be increased, the stepper motors will transfer their power through a pulley system onto the syringe systems beneath, forcing them to increase the pressure inside the cable system and therefore on to the wing. The pressure is operated by a maximum of 10 MPa in order to create enough power to operate the wings successfully against the force applied by the rock on the BHA. The deflection force was confirmed via an ANSYS simulation (**Figure 11**), taking friction losses into account, to grant the capability of the system. The simulation calculates that the system can transmit a force of 60 N onto the rock surface.
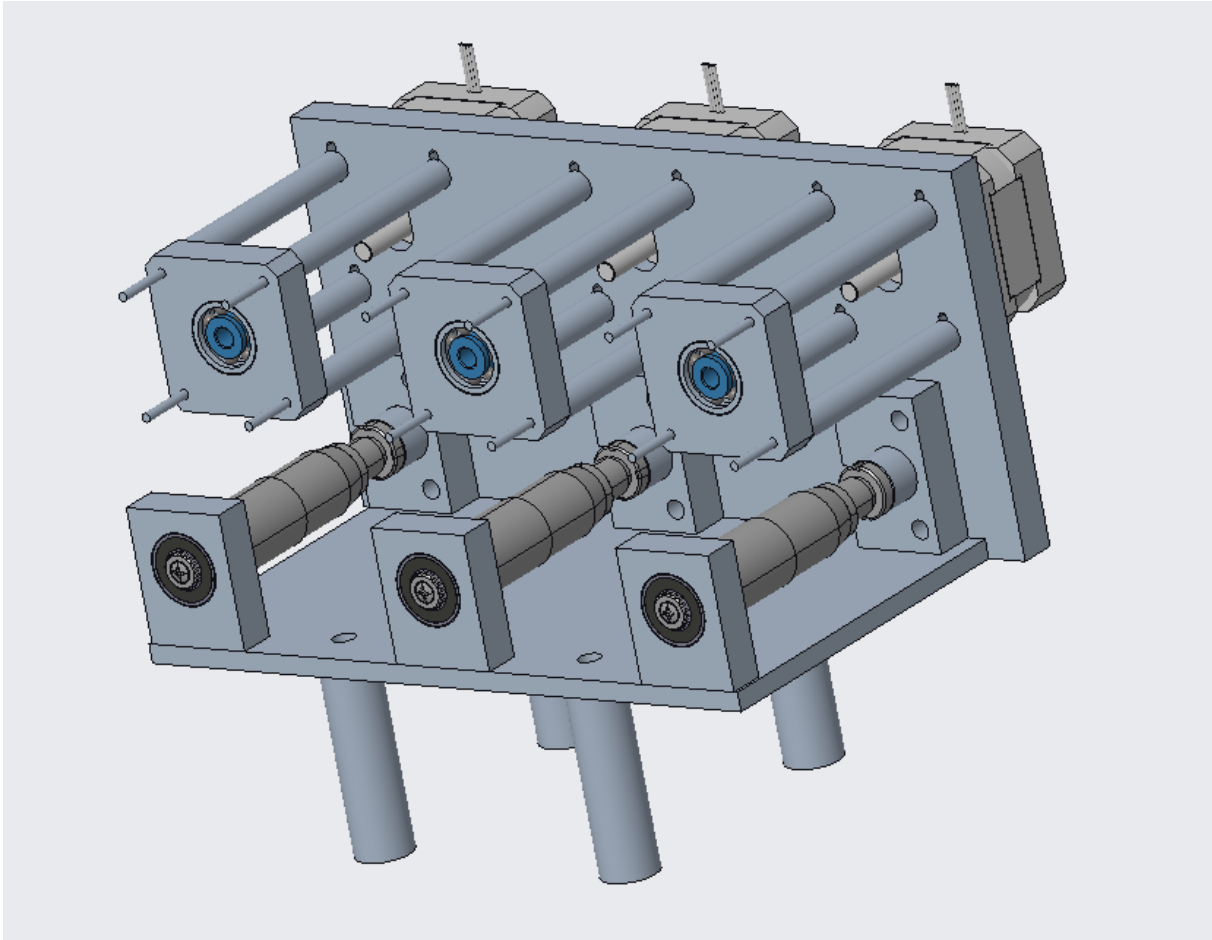
Figure 10: Syringe deflection unit
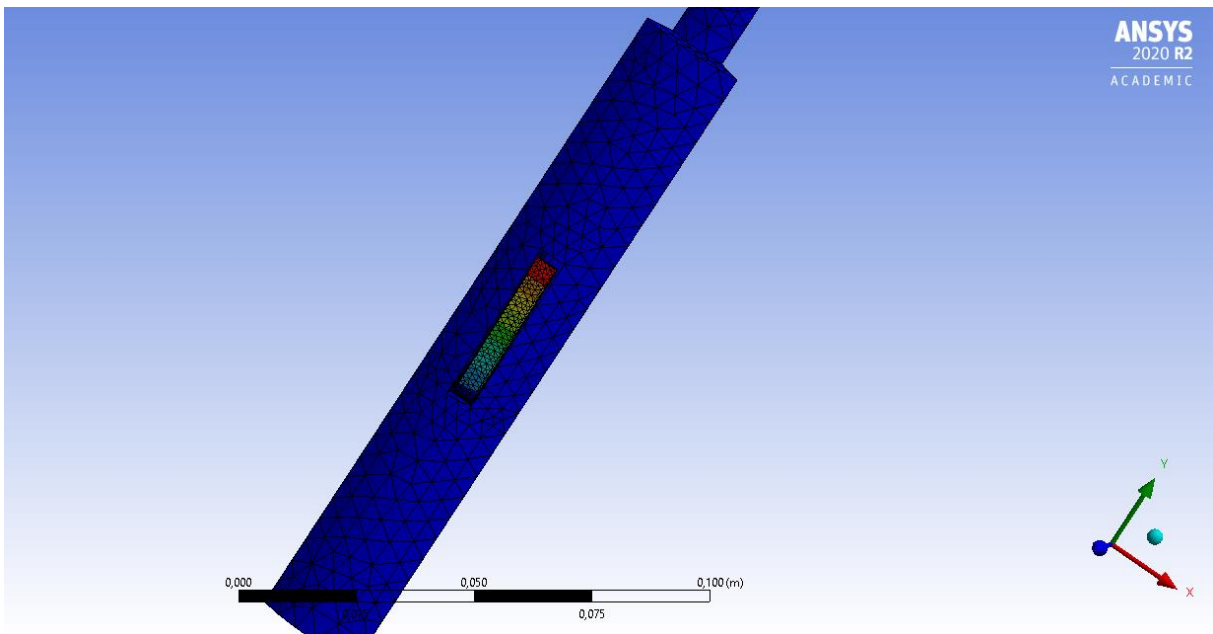
Figure 11: BHA ANSYS wing simulation

5.2.6 Maximum Inclination

With the maximum force that one wing can exert on to the rock determined by the ANSYS simulation, it is now possible to calculate the maximum deflection of the drill pipe and the BHA. A simple model was defined using a free software for structural analysis. A bar construction was defined with the respective lengths and cross sections of the drill pipe and the BHA. Density and Young's modulus for the used steel were entered. The top of the drill pipe was defined as a fixed bearing and the stabilizer as plain bearing. Finally, the acting forces were an upward force of 150 N for the maximum WOB and 60 N in x-direction for the maximum wing force. By doing that, the deflection could be computed. The result is displayed in **Figure 12**, where the bending is depicted ten times larger than the actual value for demonstration purposes. The maximum deflection at the tip of the BHA is 3.36 cm (1.3 inch).

With the maximum deflection and the length of the BHA, the maximum inclination can be calculated with

$$\varphi = tan^{-1} \left(\frac{max.\ deflection}{length\ BHA} \right) = tan^{-1} \left(\frac{3.35}{18.5} \right) = 10.3° \quad (37)$$

This model is does not count for bit-rock interaction and is only conducted under static condition. Nevertheless, it gives a good first assumption that the chosen concept and set-up can fulfil the directional drilling task.
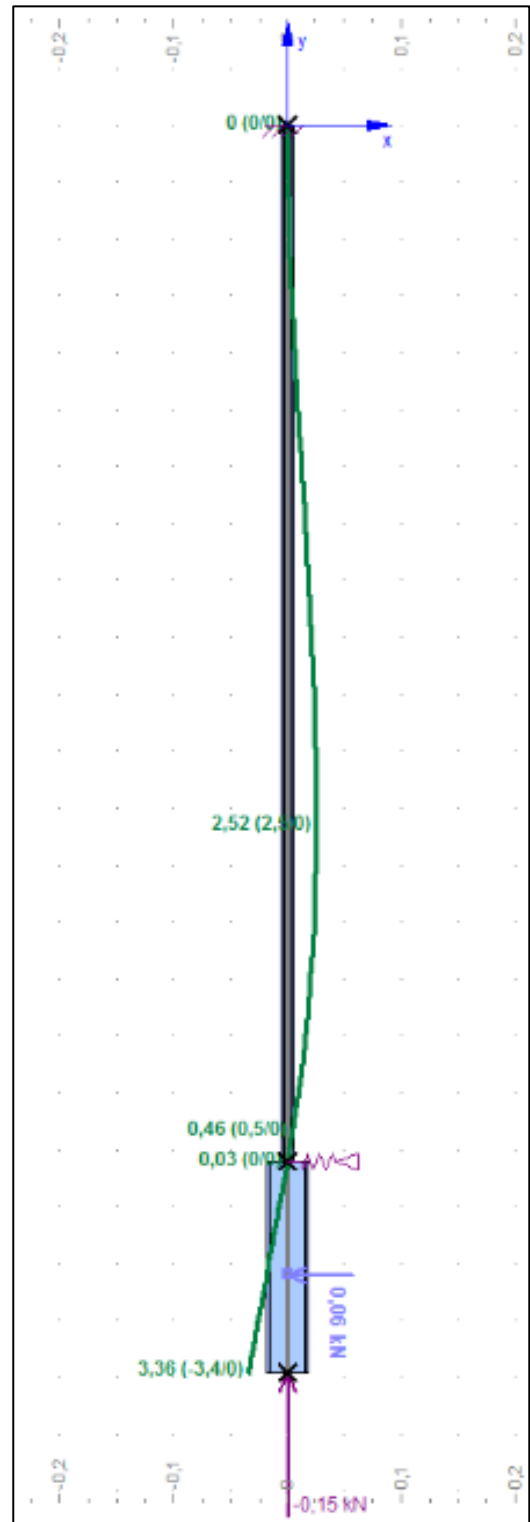
Figure 12: **Maximum deflection of the drill pipe and BHA**

5.2.7 Sensor unit

The next module connected to the upper part is the sensor unit. This unit module consists of two half circular shaped parts. The parts are mounted on the BHA beneath the steering unit and are installed in to sense the position of the Bit and the inclination of the BHA. In addition, the downhole weight on the bit is measured here, it is also possible to measure the bending moment in x and y axis and later to determine a force vector of the bit from these values. With this arrangement the actual weight on bit can be determined more precisely, as the friction of the drill pipe and the supporting moment of the BHA wings is omitted. Beneath the sensor unit the drill bit is installed. In order to meet the properties of our driving system, the System is optimized for high rpm counts and low output torque. **Figure 13** shows the whole BHA setup.
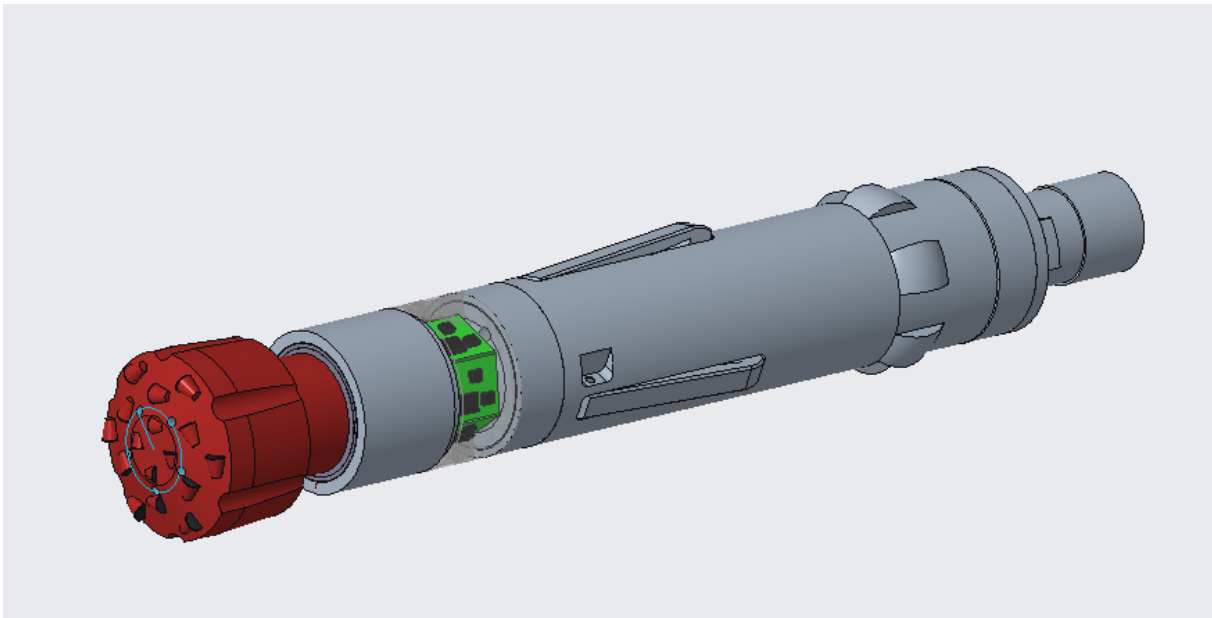
Figure 13: **BHA total setup**

5.2.8 Drill Spindle and Spindle Housing

Directly behind the drill bit, a shaft sealing ring seals the BHA from dirt and drilling fluid. The first sensor module is mounted directly behind the drill bit. This has the advantage that the drilling process can be more accurately recorded. This year´s bearing construction consists of a classic moveable/fixed bearing construction (**Figure 14**). For the two bearing rings behind the drill bit, the "fixed" bearing, the s61702-2rsr bearing was chosen. The moveable component consists of one s61700-2rsr bearing ring. These two single row ball bearings offer a great stiffness in addition to a limited requirement of installation space, which is beneficial for constructing a miniature drilling rig. Furthermore, the bearing construction can absorb the axial and lateral tilting

moments and prevents the BHA from a critical failure because of high stress moments.
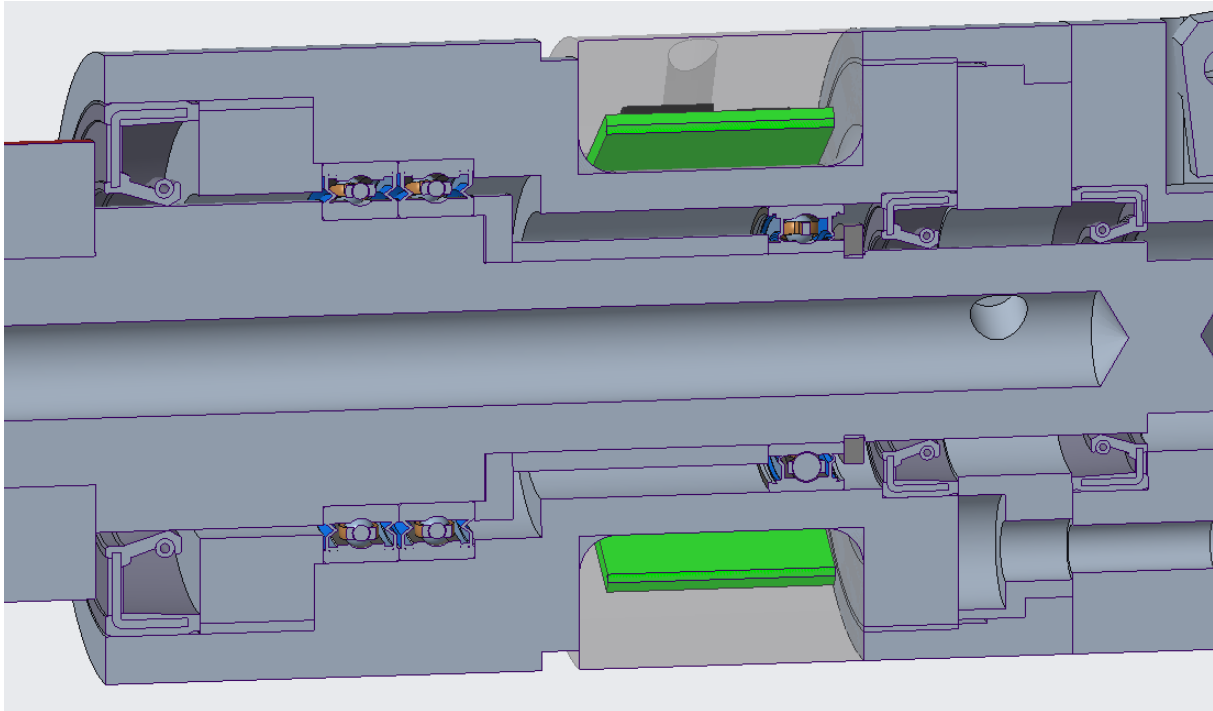
Figure 14: **Drill spindle and bearing unit**

5.2.9 Drill Bit

It was originally planned to design an own impregnated diamond drill bit to be able to drill at high RPM. But since the manufacturing of such a bit would be way bigger than initially anticipated, the decision was made to use the drill bit provided by Baker Hughes. This drill bit will deliver the necessary cutting action which is needed for the specifications of the given design.

From the two drill bits that are provided, one will be used during trials before the competition and the second drill bit will be held as a spare part in the case that the first drill bit gets damaged. In any case, the second bit will be used for the competition. The bit wear will be analyzed after each run to decide if it can be further used or not. The IADC dull bit grading system will be applied after each test run to describe the bit wear. The IADC dull bit grading system, after IADC/SPE 23938-23939, defines several parameters such as a cutting structure, bearing seals, gage, or the reason for pulling the bit. From that a conclusion can be made on the drilling performance of the bit. The wear of PDC bits is also sensitive to the amount of mud cooling the bit across its surface. Thus, it is of most importance to keep a continuous and high amount of mud flow during drilling to protect the bit of wear.

6 Mechatronic System Architecture

6.1 CAN Bus

A universal error-resistant bus system is required since many subsystems in the system are required to communicate with each other without interferences. Therefore, the decision was made in favor of the controller area network protocol, which is widely used in the automotive industry.
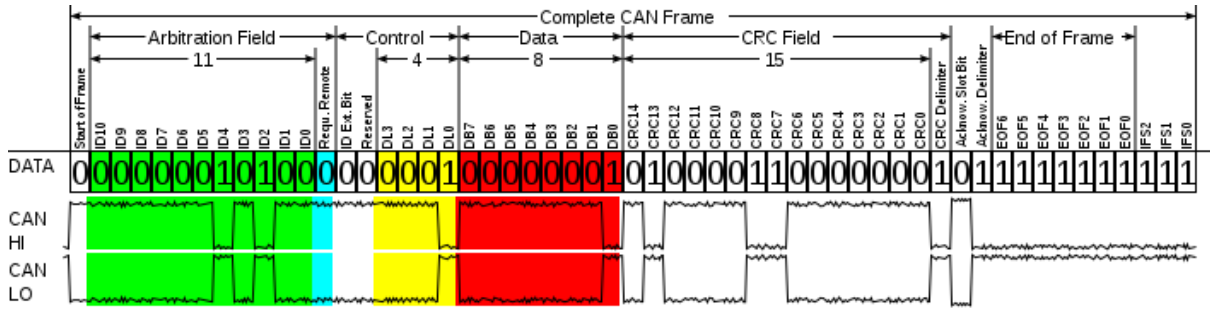
Figure 15: **CAN bus schematic**

The structure essentially consists of two redundant data lines, CAN High and CAN Low. To write one, the CAN High line goes to zero voltage while it is normally on supply voltage, the CAN Low line goes from zero voltage to supply voltage. To write a "zero", CAN High stays on supply voltage and CAN Low stays on zero voltage. This mechanism results in an opposing signal in which errors can easily be detected. In a CAN network, these two lines connect all participants. The electronics in the BHA and on the surface are also supposed to be connected in this way. Thus, actuators and sensors can exchange data with each other without a too complicated algorithm. Synchronized processes can be organized in a decentralized way. In addition, several algorithms can retrieve data and place commands in the network independently. A practical example is an initialization, or an emergency stop command. A CAN message thus consists of several sections. At the beginning there is the arbitration field which represents a sequential number. Depending on this number, only an individual module or all even modules are addressed. An emergency shutdown will have the number "1". Each module that does not receive this number will go into an error mode. This numbering also makes it possible to prioritize messages. If a sender wishes to send a message, it also listens to the bus lines simultaneously. If it randomly sends signals simultaneously with a higher priority module, it automatically stops sending and waits for a new time window. Thus, important messages are exchanged very fast. The next data field of the CAN message determines the type of message. A distinction is made between data message, the message transmits data from a module. The remote message requests data from a particular module and the error message signals

to all participants that an error condition has been triggered. The overload message forces all participants to take a pause to stabilize the data traffic. Behind it is the data field and here all data to be sent are aligned. The CAN message is terminated by a CRC, a count sum to verify the correctness of the message. If this does not agree with the sum of the message, the message is considered unusable and the data is requested again.

6.2 Quick Data Query

To transmit large amounts of data from many sensors as fast as possible, a data acquisition protocol was designed, as shown in **Figure 16.**
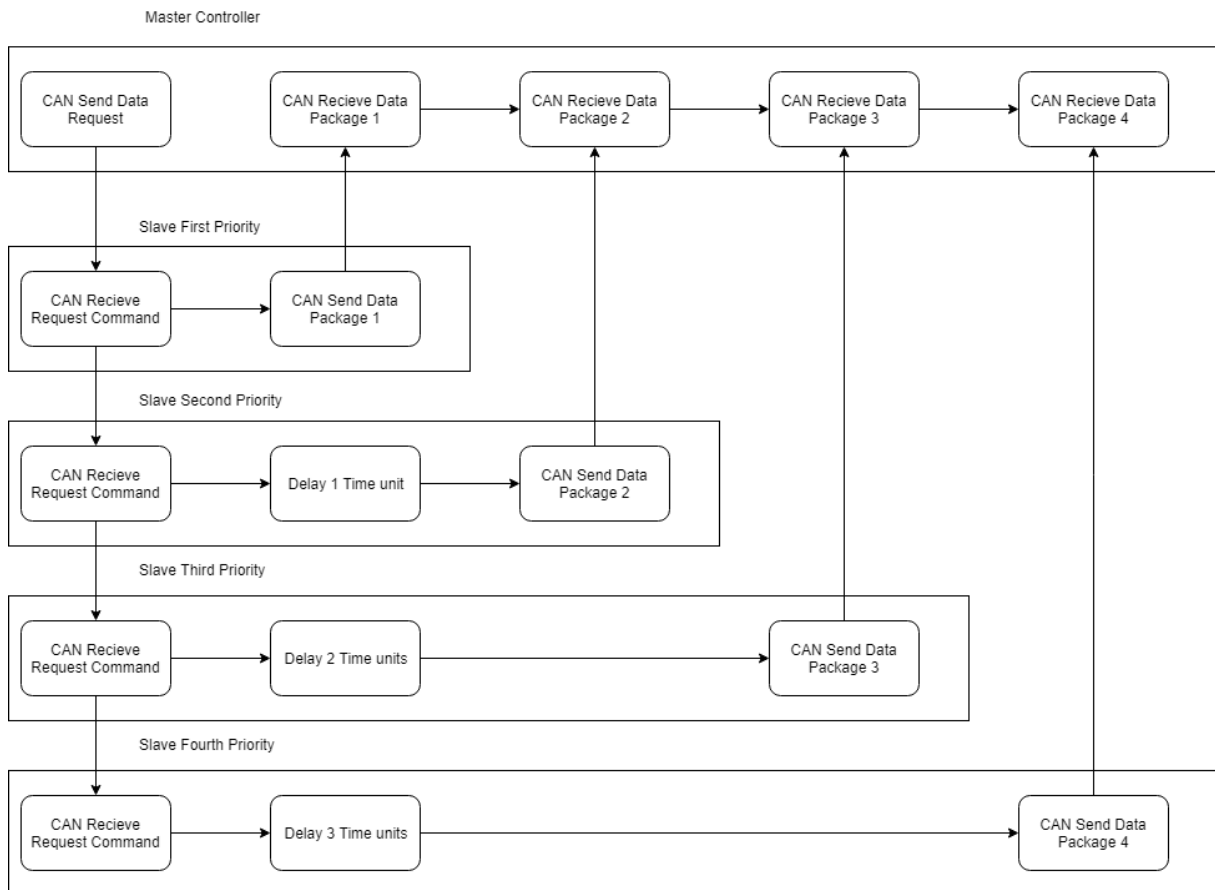
Figure 16: Quick data schematic

Normally an ECU would send a query message to a sensor and wait for a response. If this was received error-free, it would dedicate itself to the next sensor and again wait for the answer to a request. To avoid this waiting cascade, a trick is used. Each module that transmits data has a specific waiting time which corresponds to its own priority number. If a data acquisition message is imported into the network, all modules, which have no data to send,

pause their communication. All modules, at which data are to be queried, go into a "data sending mode" and wait for a specific time and, subsequently, send their data set. If this is successfully completed, the network returns to normal operation. Thus, the time required for the normal polling can be saved.

6.3 Actuator Modules

6.3.1 Motor Control Unit
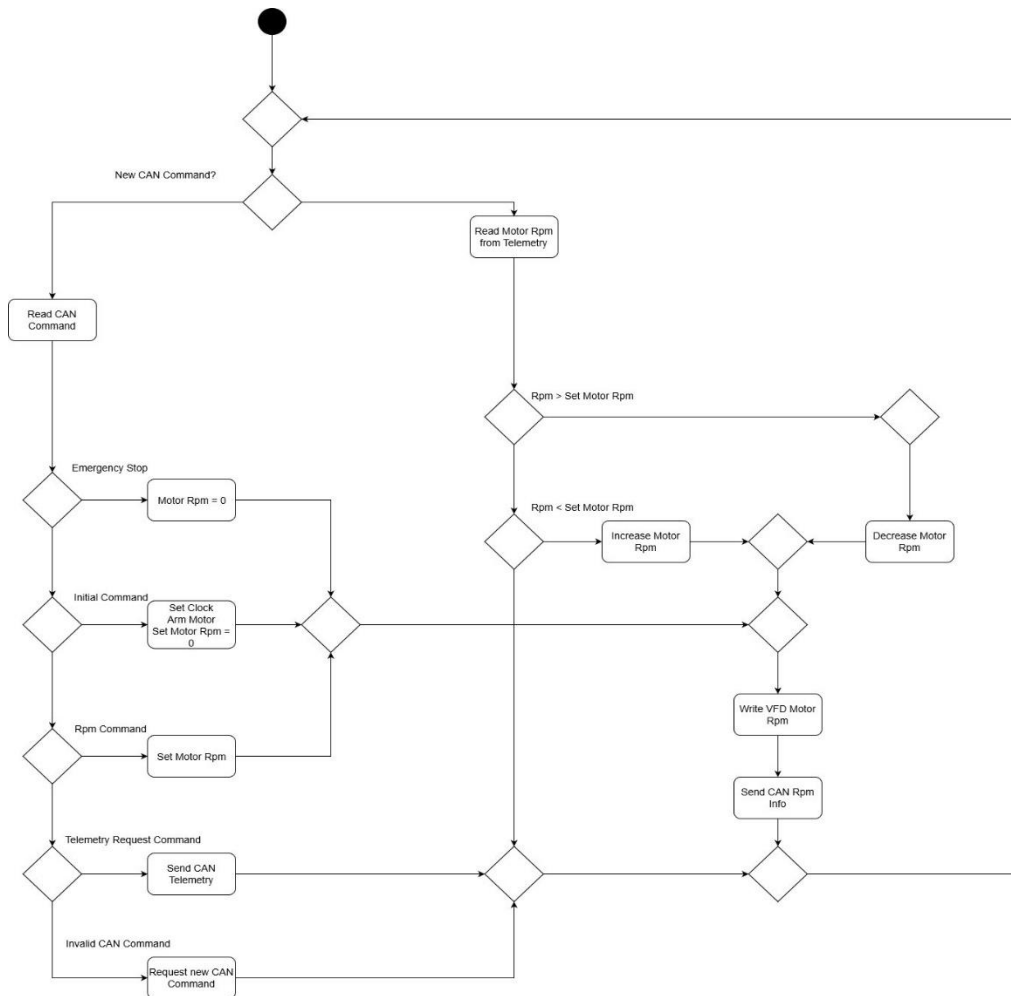
Figure 17: **Motor control algorithm**

The motor control unit consists of several parts as shown in **Figure 17** and is located on the surface at the top of the spindle. The STM32 will process the information of the motor controller and has a CAN interface for bidirectional communication with the CAN bus.

To adjust the required speed of the main system, a small control loop runs on the STM32 as shown in the **Figure 18**. If the current speed is lower than required, the signal is amplified to increase the RPM, however, if the speed is too high, the control signal is reduced. In case the system requires data, current, voltage, speed and set control signal as well as temperature will be

sent back. The motor controller is a variable frequency drive (VFD), which can control the speed of the BLDC motor by adjusting the frequency and voltage. Because the motor is mounted outside the BHA, no additional temperature sensor and cooling system are required. As an alternative to the VFD, an electronic speed control (ESC) is considered
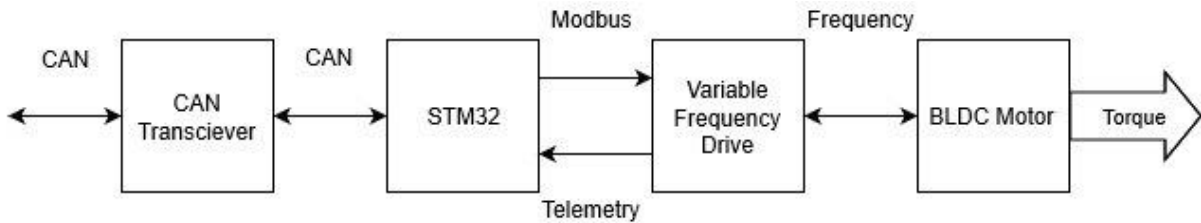
Figure 18: **Motor control unit**

Communication between the microcontroller and the motor controller takes place via Modbus. Modbus is a communication protocol that allows data exchange between a master and several slaves. The master device, the STM32, is connected to the slave device, the control unit. The Modbus protocol now allows the control of the connected devices and the transmission of the measurement data from the slave to the master. Basically, each participant can send messages via the bus, where a communication is usually initiated by the master.

6.3.2 Hydraulic Actuator Unit
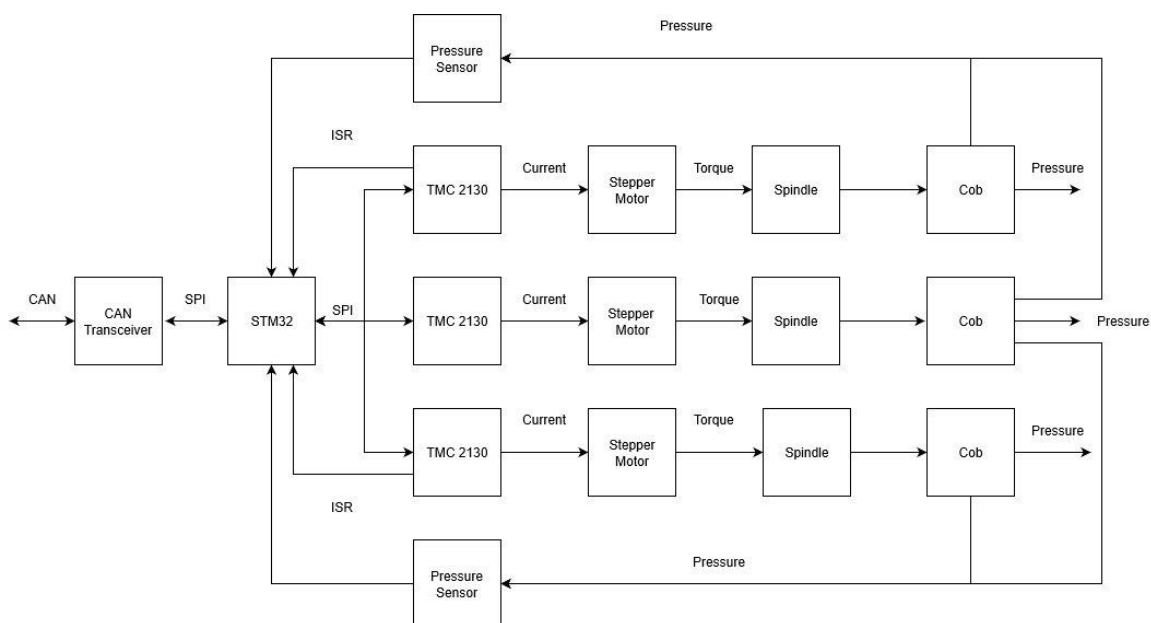
Figure 19: **Hydraulic actuator unit**

The steering unit is controlled by three offset wings, which are extended by a hydraulic system and controlled by adjusting the pressure as shown in the **Figure 19**. For each wing there is an associated stepper motor and stepper motor driver. The TMC2130 regulates the motors by adjusting the current. The stepper motors transmit a moment to the spindle, which in turn moves a cob that adjusts the pressure in the chamber. The deflection of each wing can be adjusted by the number of steps of the motor. The pressure within the system is measured with a pressure sensor and the data is passed on to the STM32. The microcontroller communicates with the pressure sensors and the TMC2130 via SPI. The STM32 transfers the data via CAN to the transceiver and further on the CAN bus. Each stepper motor driver possesses an interrupt service routine (ISR) which is triggered in the event of an interrupt request. The interrupted program is then continued where it has been interrupted.

6.3.3 Rotary Table Control

The rotary encoder control unit, as seen in the **Figure 20**, consists of a CAN transceiver and an STM32, which controls a stepper motor driver and assesses the absolute rotary encoder. The unit also features a digital thermometer.
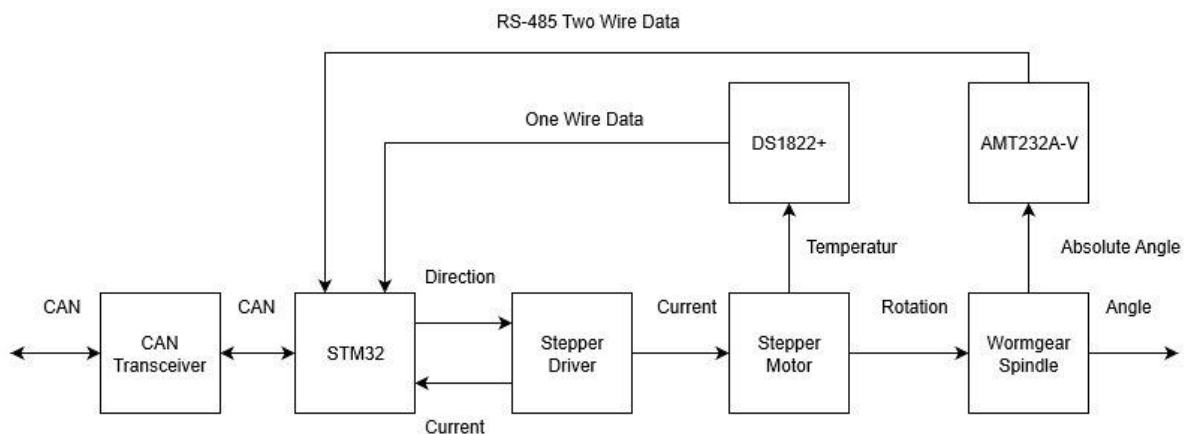
Figure 20: **Rotary table control unit**

The algorithm determines the current angle value and compares it with the desired angle. If a deviation is determined, the system moves in the opposite direction to correct the deviation to zero. As soon as the stepper motor moves, the temperature and the motor current are additionally determined and compared with a previously defined maximum value. As soon as these values are exceeded, a warning message is generated.

6.3.4 Hoisting System Control Unit

This unit consists of a CAN transceiver and an ATMEGA 328p as well as switching inputs for the upper and lower limit switch of the hoist axis.
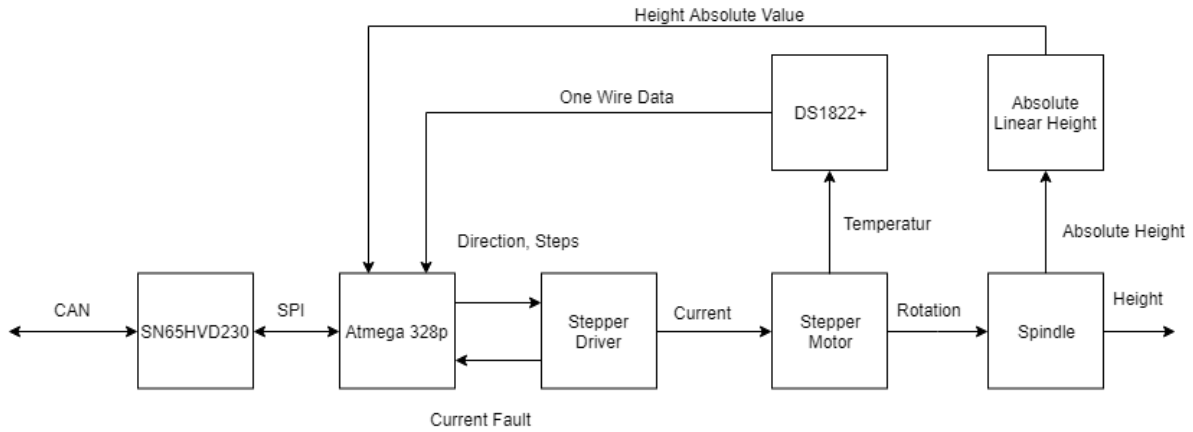
Figure 21: **Hoisting system control unit schematic**

The algorithm has in total two modes. In the first mode, N steps are driven in the pre-set direction. The second mode moves to a desired WOB and adjusts it with the hook load via the spindle. Since the controller has access to the data of the Downhole WOB module via CAN network, abnormal operating states can be determined by a comparison.

6.3.5 Relay Switching Unit

The mechatronic system contains a CAN network controllable relay card which switches the pump. This unit consists of an ATMEGA 328p and a CAN transceiver as well as a relay card. In addition, a pressure sensor and a flowmeter are added to the pump control system, with which the values of the system can be checked.

6.4 Sensor Units

6.4.1 MWD Sensor unit

To enable a quick change in the event of a fault, the sensor unit is standardized. Two identical sensor units, which consist of a magnetometer (LIS3MDL) and an accelerometer (LSM6DS33), are used and attached to both the upper and lower notches of the BHA. As shown in the **Figure 22**, one central microcontroller is used for each sensor. Communication between the sensors and controller is via SPI. The information is processed by the STM32 and transmitted to the transceiver via CAN communication. This forwards the data to the bus via a CAN protocol. With this design, the magnetic range magnetometer can use the magnetic field strength outside the BHA. To ensure that the data is measured and transmitted as accurately as possible, a Madwick filter is implemented.

The sensor unit consists of three smaller circuit boards arranged inside the sensor ring. The system consists of a power cell that supplies the entire unit with power. For this purpose, two voltage regulators are installed to regulate

the voltages for the electronics down to 5V and 3.3V respectively. This board is standardized and used for all sensors. The microcontroller, the sensors and the CAN transceiver are mounted on another board which is in the middle of the ring facing the inside. In addition, a standardized USB Type C connector is used, which is intended for data transfer and programming the STM32. The new connector is point-symmetrical and can be plugged in both possible orientations. Another advantage of the Type-C connector is a low height and low width of the socket.
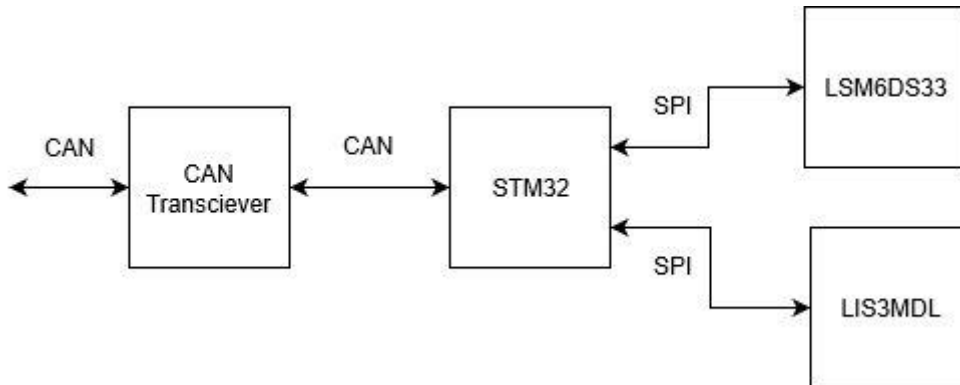
Figure 22: **Electrical schematic of the Sensor Unit**

The sensor unit in the lower notch of the BHA will be located over the drill bit. Since the BHA is constantly flooded, it is necessary to shield the sensors from water or make them waterproof. Therefore, the two sensor modules are framed with epoxy resin or silicone. The plugs are laid from the housing to the inside, where the cables are also guided along. Another sensor unit is placed at the upper end of the BHA. The two rings make it possible to better determine references and deflections of the entire BHA. In addition, another accelerometer is implemented within the BHA to measure and filter out the vibrations.

Another identical sensor unit is attached to the drill pipe to measure the vibration of the drill string. These values are included in the control algorithm. This allows a maximum value to be set at a point that must not be exceeded. If the value is exceeded an alarm the RPM of the flexible shaft will be reduced. If an even higher threshold is reached, the drilling process will be stopped for safety considerations.

6.4.2 WOB Measurement Unit

The Downhole WOB is measured by a strain gauge inside the BHA. The unit has an ADS1261 analog digital converter and a CAN transceiver which is controlled by a STM32 microcontroller. On request, the unit returns a WOB value or warning message if the set maximum value is reached or exceeded.
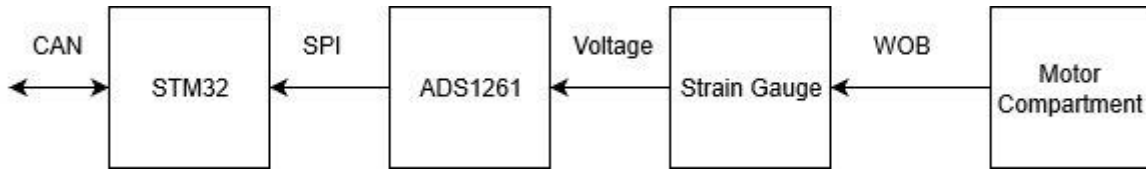
Figure 23: **WOB Measurement module schematic**

The measuring strips are placed on the housing above the bit. The aim is to include both elongation and torsion values. Due to the very small output values, an amplifier is needed. The ADS1261 has an internal signal amplifier which passes the amplified and converted output signal to the STM32 and finally forwards it to the bus via CAN. In the sensor module, the measuring strips are mounted as a full bridge and half bridge as shown in **Figure 24** and **Figure 25** respectively. Due to this arrangement, suitable values can be included, and the temperature influence on the strips is compensated. Both the sensors and the strain gauges will be provided with their own microcontroller, which will be applied to a standardized breakout board. On both STM32 loops will run and query data permanently.
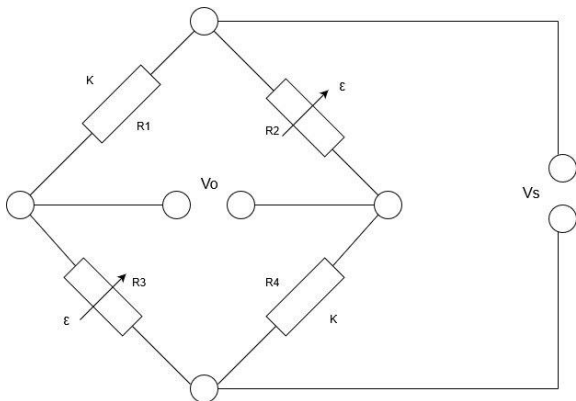
Figure 24: **Wheatstone Half-Bridge**
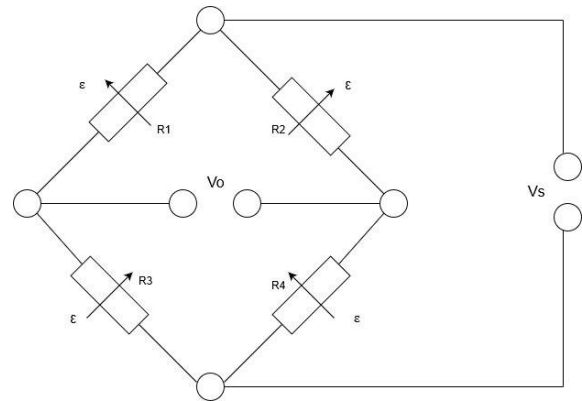
Figure 25: **Wheatstone Full-Bridge**

For measuring normal elongation, the strain gauges are arranged as a diagonal bridge, each with 2 active and 2 passive measuring strips. This measures normal elongation independently of the bending strain. The strain is described by the following formula:

$$\varepsilon = \varepsilon_n = \frac{1}{2} \cdot \frac{4}{k} \cdot \frac{V_0}{V_s} \qquad (38)$$

Where k is the K-factor of the measuring strips and Vs and Vo are the adjacent voltages. The equation can calculate the change in length that can be compared with the previously determined real values to find the critical values.

To measure the torsion, the strain gauges are installed as a full bridge, with four superimposed strips offset by 45°. The principle is like that of the half bridges and is described by the following formula:

$$\varepsilon = \varepsilon_d = \frac{1}{4} \cdot \frac{4}{k} \cdot \frac{V_0}{V_S} \qquad (39)$$

6.4.3 RPM Measurement

To capture the rotations of the shaft, a 1-bit encoder in the form of an infrared or light sensor is provided. For this purpose, a part of the shaft is colored so that it is perceived by the sensor. The output of the sensor will be given as a rectangular signal, which allows to determine the number of rotations by the measured pulses.
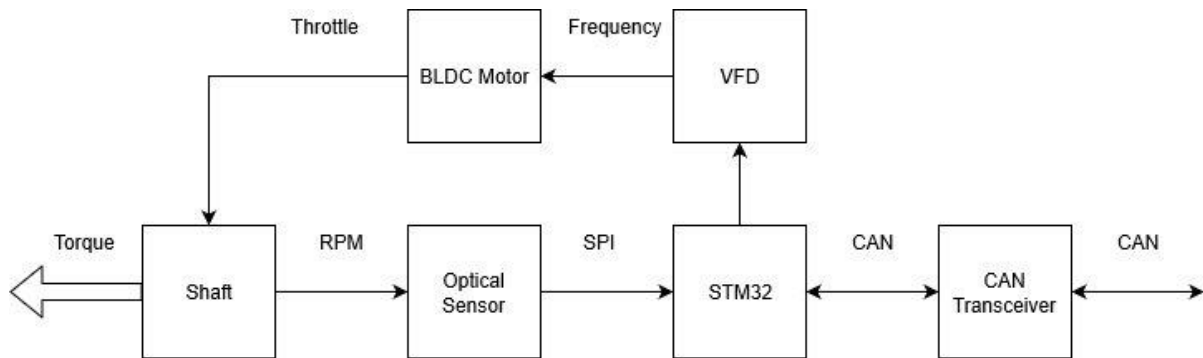
Figure 26: **RPM measurement**

6.5 Sensor Calibration

6.5.1 Accelerometer

The calibration process of the accelerometer involves two steps. These steps should eliminate the scale factor error $o_{x,y,z}$ and the bias offset $s_{x,y,z}$. The bias offset is a simple offset of the initial zero position of the sensor. The scale factor error on the other hand describes a deviation between the input and the output of the sensor.

These influences can be eliminated by pointing the x-axis towards the earth. The maximum read values of the sensor should then be used to calculate the bias offset error and the scale factor error for both negative and positive directions.

$$o_x = \frac{x_{max} + x_{min}}{2} \qquad (40)$$

$$s_x = \frac{x_{max} - x_{min}}{2} \qquad (41)$$

44

The calibrated value can then be calculated by the following formula:

$$a_{x,corrected} = \frac{a_{x,measured} - o_x}{s_x} \qquad (42)$$

This process should be repeated for all axes of the sensor unit.

6.5.2 Gyroscope

Like the accelerometer the gyroscope needs to eliminate the bias offset and the scale factor error. However, the calibration approach differs in comparison to the other sensor. The bias offset $o_{x,y,z}$ of the gyroscope shifts after every restart which makes a static value for the bias offset useless. Therefore, the gyroscope needs a static starting sequence, where a certain amount of measurements is taken and averaged for all three axes. These averages can then be subtracted from the actual measurement to obtain the bias offset compensated value.

$$s_x = \frac{x_{max} - x_{min}}{2} \qquad (43)$$

The compensation of the scale factor error $s_{x,y,z}$ is done by measuring the peak values of the gyroscope while its rotating around the x-axis at its maximum speed in both directions. The peak values during the maximum turning rate will be measured to calculate the scale factor error.

$$s_x = \frac{x_{max} - x_{min}}{2} \qquad (44)$$

The corrected characteristic curve of the gyroscope can then be calculated by the following formula:

$$\Omega_{x,corrected} = \frac{\Omega_{x,measured} - o_x}{s_x} \qquad (45)$$

The last influence that must be measured, which is not part of the actual calibration procedure, is the angular drift over time (also called bias stability). The bias stability value is important for the calculation of the gains β and ζ in the MARG Filter in chapter 6. This influence will be measured once with the help of the Allan variance method. With this method noise influences in gyroscopes and other angular rate sensors can be evaluated. Moreover, this method can be helpful to compare the performance increase of the sensor output after applying different filters on it and thus will be helpful for future adaptations of the sensor algorithm.

6.5.3 Magnetometer

The calibration process of the magnetometer is somewhat comparable to the other two sensors but to understand these compensation methods one must look at the causes of the disturbances and why some disturbances cannot be corrected with the usage of filters and calibration procedures.

The first possible error sources are 'Hard-Iron' interferences. These interferences emerge from static magnetic fields created by close by ferromagnetic objects or magnets. However, this error will simply act as an offset error $o_{x,y,z}$ which can easily be taken care of. This offset can be calculated by measuring the peak values for each axis in the negative and positive direction of the earth's magnetic field.

$$o_x = \frac{x_{max} + x_{min}}{2} \quad (46)$$

Secondly disturbances can arise from 'Soft-Iron' interferences. These influences distort the magnetic field and arise from nearby non-magnetic materials. These distortions can be adjusted with a proper rotation matrix which aligns the distorted measurements with the earths reference frame.

The last possible negative influences for the sensor performance are dynamic magnetic fields. These can be emitted from electric devices such as DC motors and are not possible to compensate in this algorithm. Therefore, the influence of these dynamic fields is avoided by placing the sensor as far away as possible.

6.5.4 Strain gauge

The calibration process of the strain gauges for the measurement of the WOB and the hook load are quite simple. To accurately measure forces with strain gauges an adequate bridge circuit should be chosen to for example compensate temperature influences (as seen in chapter 6.3.2 WOB measurement unit).

Since the voltage output of the strain gauges and the acting forces are proportional to each other, the calibration process of the strain gauges only needs two different measurements to accurately display the forces. One measurement must be taken in a static situation where no forces are applied, and the next measurement must be taken while a known force is applied to the strain gauge.

$$p_{prop} = \frac{F_{known} - F_0}{V_{known} - V_0} \quad (47)$$

With these measurements the proportionality factor p_{prop} between the acting forces and the voltage output can be calculated. The same procedure can be applied to measure acting torque on the strain gauges.

If applying a force or torque is not applicable for the placement of the strain gauges, a shunt calibration method can also be used.

7 Data Handling

7.1 Synchronization

To achieve a nearly synchronous timing on the whole rig between all modules on the Can Bus a synchronization message was introduced. The main controller sends this message to the Can network during initialization before the actual drilling process and each module sets its own millisecond timer to zero. In this way a clocked interaction of the modules can be achieved, and time critical tasks can be better managed. As soon as the drilling process starts, the can messages are stored on the recording module with this timestamp in milliseconds and the actual time.

7.2 Filter

The MARG filter used for the combination of the tri-axis accelerometer, magnetometer and gyroscope data is an efficient combination of compensation and heading algorithms which can compete with similar methods for IMU sensors like a Kalman-filter approach. This filter will only be explained briefly in this report since a deep explanation and discussion was already made by its creator Sebastian O. H. Madgwick in 'An efficient orientation filter for inertial and inertial/magnetic sensor arrays'.

First and foremost, to understand the working principle of the algorithm one must look at the different methods of rotating different coordinate reference frames. This is important since the coordinate system of the sensor system will most certainly not align with the desired reference system of the drilling rig. This rotation of reference frames can be achieved by either the Euler method, which is considerably easier to understand, and the Quaternion approach. The Quaternion based method was chosen since it was already used in the depicted filter algorithm in **Figure 27**.

The Quaternion based method is essentially an expansion of the complex number System to make it applicable to three-dimensional problems. This is represented by extending the complex numbers from one imaginary part $b \cdot \boldsymbol{i}$ to three imaginary parts represented by $b \cdot \boldsymbol{i}$, $c \cdot \boldsymbol{j}$ and $d \cdot \boldsymbol{k}$.

$$q = \underbrace{a}_{Real} + \underbrace{b \cdot i + c \cdot j + d \cdot k}_{Imaginary} \qquad (48)$$

This method is preferred in comparison to the Euler approach since the rotation of a reference frame with a Quaternion based method can be done by the Quaternion product. This Quaternion product, denoted by the operator $\otimes$, uses only basic arithmetic operations like subtractions and multiplications. This results in a considerably faster operating speed compared to the rotation matrix used by the Euler method which relies on trigonometric functions like sine and cosine.
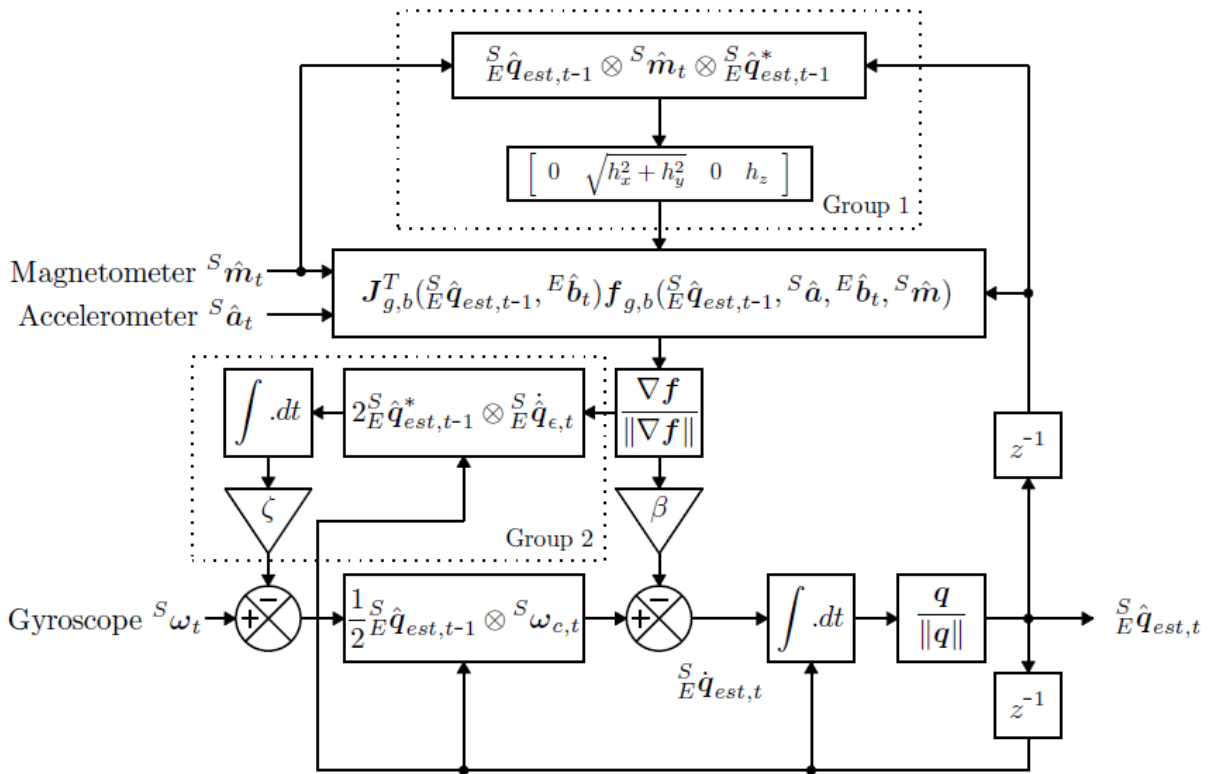
Figure 27: **Block diagram of the MARG-Filter with gyroscope drift and soft iron distortion compensation modules**

The block diagram depicted in **Figure 27** explains the working principle of the MARG filter in a compact manner. The unfiltered measurements of the Magnetometer ${}^{S}\hat{m}_t$ and accelerometer ${}^{S}\hat{a}_t$ enter the block with the functions $J_{g,b}^T\left({}^{S}_{E}\hat{q}_{est,t-1}, {}^{E}\hat{b}_t\right)$ and $f_{g,b}\left({}^{S}_{E}\hat{q}_{est,t-1}, {}^{S}\hat{a}_t, {}^{E}\hat{b}_t, {}^{S}\hat{m}_t\right)$. This block basically describes the function gradient ∇f of the magnetometer and accelerometer measurements. This is needed as a part of the gradient descent algorithm which is used to align the sensor frame S with the earth frame E. For the first iteration of this algorithm the term ${}^{S}_{E}\hat{q}_{est,t-1}$ needs an initialization value. This value will be set to ${}^{S}_{E}\hat{q}_{est,0} = [1,0,0,0]$.

The block above the function gradient ∇f (highlighted by the dotted box 'Group 1') is solely used to compensate the soft iron influences on the measurements of the magnetometer by rotating the magnetometer measurements $^S\hat{m}_t$ by the estimated orientation of the sensor $^S_E\hat{q}_{est,t-1}$ (the index * denotes the conjugate of a Quaternion which is similar to the conjugate of a complex number and describes a rotation in the opposite direction). This rotated vector $^E\hat{h}_t$ then needs to be adjusted for inclination errors. This is done by normalizing the values h_x and h_y of the vector $^E\hat{h}_t$. The newly constructed vector $^E\hat{b}_t$ only uses the previously calculated norm and the h_z values for the earths frame in the x and z axis.

The lower half of the algorithm shows that the gyroscope measurements $^S\omega_t$ enter a summation block where the gyroscope bias drift error $^S\omega_{b,t}$ is subtracted from the actual measurements $^S\omega_t$. The block outlined with the description 'Group 2' shows the working principle of this compensation method. To accurately estimate the orientation error, one must use the norm of the gradient function $\frac{\nabla f}{\|\nabla f\|}$ of the magnetometer and accelerometer data. This value represents the rate of change in orientation $^S_E\hat{\dot{q}}_{\epsilon,t}$. After that the product of $^S_E\hat{\dot{q}}_{\epsilon,t}$ and $^S_E\hat{q}^*_{est,t-1}$ needs to be integrated. This calculation leads to the DC component $^S\omega_t$ of the bias error. This error then needs to be subtracted from the actual measurements with an appropriate gain ζ. The result of these subtractions are gyroscope measurements $^S\omega_{c,t}$ which will not be influenced by an overtime increasing drift. After that the corrected gyroscope values must be rotated towards the earths current reference frame $^S_E\hat{q}_{est,t-1}$.

The actual fusion of all three sensor measurements occurs in the lower half of block diagram. The normalized rate of change of the magnetometer and accelerometer $\frac{\nabla f}{\|\nabla f\|}$ is multiplied by the factor β which describes the divergence rate of the gyroscope. This product is then subtracted from the drift free gyroscope measurements $^S_E\dot{q}_{\omega,t}$. The result then needs to be integrated to get the current heading. After that the unit quaternion $\frac{q}{\|q\|}$ must be calculated. This last operation leaves the user with a unit quaternion of the current heading of the sensor $^S_E\hat{q}_{est,t}$ which will then be used for the next iteration to update the current heading to repeat the process (this is represented by the block z^{-1} which is the conjugate of the unit Quaternion $\frac{q}{\|q\|}$).

These Quaternions then must be transformed into useable representations which would be Euler angles. These transformations can be done by the following formulas:

$$\psi = atan2(2bc - 2a, 2a^2 + 2b^2 - 1) \quad (\textbf{49})$$

$$\theta = -sin^{-1}(2bd + 2ac) \quad (\textbf{50})$$

$$q = atan2(2cd - 2ab, 2a^2 + 2d^2 - 1) \quad (\textbf{51})$$

The function atan2 in the above-mentioned **Equations 49** and **10** describes an expansion of the inverse of the tangent function. This function needs two real arguments with which it can calculate an angle in the complete range of 360 degrees.

In consideration for a performance increase of the sensor are an additional low pass filter (or other high frequency suppressing filters) to decrease the influence of vibrations of the accelerometer measurements $^S\hat{a}_t$. However, to accurately program the low pass filter, the cut off frequency needs to be estimated which can only be done after measurements have been taken with the drilling rig.

7.3 Trajectory Calculation and Control Algorithm

For path estimation and controlling disturbances we used the paper of Zhang et al. as guidance. This was chosen over our previous setup that we developed from scratch since this was a more sophisticated concept that didn't need additional development time. However, if time is still available in the development phase, we will try to implement the previous concept of using piecewise hermite interpolation pylonomials for trajectory calculation and develop our own control algorithm to follow this trajectory accurately.

Before the actual algorithm can be explained we need to define a few values. First, we need the maximum support force F_{max} and the minimum support force F_{min} of the three wings used to steer the drill bit. Secondly the maximum usable steering force A_{max} must be calculated as well as the maximum dogleg γ_{max}.

$$A_{max} = \frac{\sqrt{3}}{2} \cdot (F_{max} - F_{min}) \quad (\textbf{52})$$

After that the actual trajectory calculation of the desired path can begin. This calculation can be summarized by the following **Figure 28**.
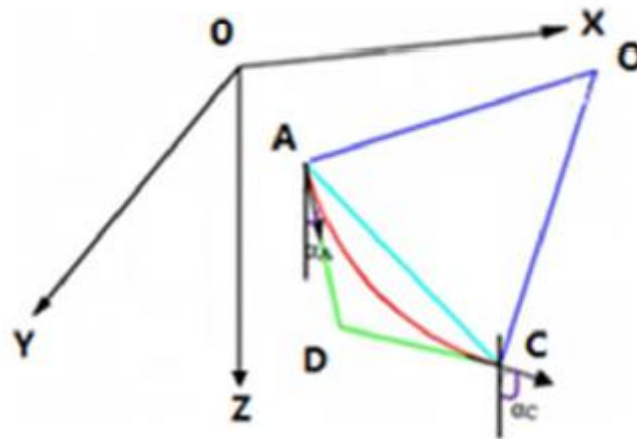
Figure 28: Starting point A and desired point C

To estimate the path between the given starting point A (given by the coordinates X_A, Y_A, Z_A) and the desired target point C (given by the coordinates X_C, Y_C, Z_C) one must simply calculate a constant radius between the points A and C. Additionally the angles of the starting point A (α_A and β_A) and the target point (α_C and β_C) must be calculated which can be done by using the tangent of the point in relation to the given reference frame. This procedure can be applied to several desired points to estimate the complete trajectory for an infinite amount of reference points.

With these factors known the amplitude of the steering force A_k can be calculated. To determine that we need the delta of the angle of inclination $\Delta\alpha_{AC}$ and the delta of the azimuthal angle $\Delta\beta_{AC}$ as well as an average inclination angle α_0.

$$\Delta\alpha_{AC} = \alpha_C - \alpha_A \qquad (53)$$

$$\Delta\beta_{AC} = \beta_C - \beta_A \qquad (54)$$

$$\alpha_0 = \frac{\alpha_A + \alpha_C}{2} \qquad (55)$$

After that the current dogleg γ can be calculated as follows:

$$\gamma = \frac{30 \cdot 360 \left| sin\left(\frac{\sqrt{\Delta\alpha_{AC}^2 + \Delta\beta_{AC}^2 \cdot sin(\alpha_0^2)}}{2} \right) \right|}{\pi\sqrt{(X_C - X_A)^2 + (Y_C - Y_A)^2 + (Z_C - Z_A)^2}} \qquad (56)$$

With both the current and maximum dogleg known, we can estimate the amplitude of the required steering force A_k.

$$A_k = \frac{\gamma}{\gamma_{max}} \cdot 100\% \qquad (57)$$

After the calculation of A_k we can calculate the direction of the steering force α_k. For that we first must calculate the expected build rate $\Delta\alpha$ and the expected walk rate $\Delta\beta$. The variable ΔD_m in the following formulas describes the vertical depth between the points C and A in **Figure 28**.

$$\Delta\alpha = 30 \cdot \frac{\alpha_C - \alpha_A}{\Delta D_m} \qquad (58)$$

$$\Delta\beta = 30 \cdot \frac{\beta_C - \beta_A}{\Delta D_m} \qquad (59)$$

With these values known we can calculate α_k. However, first we must differentiate between 9 cases (for the exact 9 cases please refer to Zhang et al.). To determine which case is used to estimate the correct angle we must take the expected build $\Delta\alpha$ and walk rate $\Delta\beta$ into account.

With the needed direction of the control force now known we can calculate the actual force F_i which is needed for all three wings. To calculate these forces the following two equations are given:

$$F \cdot cos(\alpha_k) = F_1 \cdot cos(\alpha_1) + F_2 \cdot cos(\alpha_1 + 240) + F_3 \cdot cos(\alpha_1 + 120) \qquad (60)$$

$$F \cdot sin(\alpha_k) = F_1 \cdot sin(\alpha_1) + F_2 \cdot sin(\alpha_1 + 240) + F_3 \cdot sin(\alpha_1 + 120) \qquad (61)$$

Since we need three variables and only have two equations, we cannot solve this problem with the given information. Therefore, the paper suggests setting one of the wings to maximum or minimum possible force. To determine which of these wings will be set to this value and if the force is maximum or not the system is divided into six sections for the azimuthal angle.

The steering force is either in direction of the wings (favorable area f) or in the exact opposite direction (unfavorable area uf). Since all the six sections are equal in size, the tolerances for these areas are ±30°. To determine the missing third equation, the paper suggests that if the directional force lies in a favorable area the force F_i is equal to F_f and if it lands in an unfavorable area F_i is equal to

F_{uf}.

The forces F_f and F_{uf} are calculated as follows:

$$F_f = \frac{F_{max} + F_{min}}{2} + \frac{F_{max} - F_{min}}{2} A_k \qquad (62)$$

$$F_{uf} = \frac{F_{max} + F_{min}}{2} - \frac{F_{max} - F_{min}}{2} A_k \qquad (63)$$

It needs to be noted that an initial condition is needed for the start of the algorithm where F_i is equal to the initial force F_{ini}.

$$F_{ini} = \frac{F_{max} + F_{min}}{2} \qquad (64)$$

At last we calculate the relative direction of the steering force α_k'. The resulting value can be divided into the two following results.

$$\alpha_k' = \begin{cases} \alpha_k - \alpha_1; \ \alpha_k \geq \alpha_1 \\ \alpha_k - \alpha_1 + 360; \ \alpha_k < \alpha_1 \end{cases} \qquad (65)$$

To calculate the actual forces F_1, F_2 and F_3 of the wings we divide the calculations into six different cases which depend on the actual value of α_k' (for the exact six cases please refer to Zhang et al.).

With the forces F_1, F_2 and F_3 now known we need to calculate the actual force that is needed to move the hydraulic pistons. The piston forces F_{ki} depend on the wing position and the required wing contact force. By means of the geometrical relations the pivot angle φ_i can be calculated as a function of the piston position via an approximate function (polynomial). With the help of the pivot angle the necessary piston force can be calculated to achieve the required wing contact force.

$$F_{k1} = \frac{F_1 \cdot L_{k0} \cdot cos(\varphi_1)}{cos(\beta_1) \cdot R} \cdot sin(\beta_1 + \varphi_1) \qquad (66)$$

$$F_{k2} = \frac{F_2 \cdot L_{k0} \cdot cos(\varphi_2)}{cos(\beta_2) \cdot R} \cdot sin(\beta_2 + \varphi_2) \qquad (67)$$

$$F_{k3} = \frac{F_3 \cdot L_{k0} \cdot cos(\varphi_3)}{cos(\beta_3) \cdot R} \cdot sin(\beta_3 + \varphi_3) \qquad (68)$$

For the entire step by step explanation of the **Equations 66, 67** and **68** please refer to **Appendix D**.
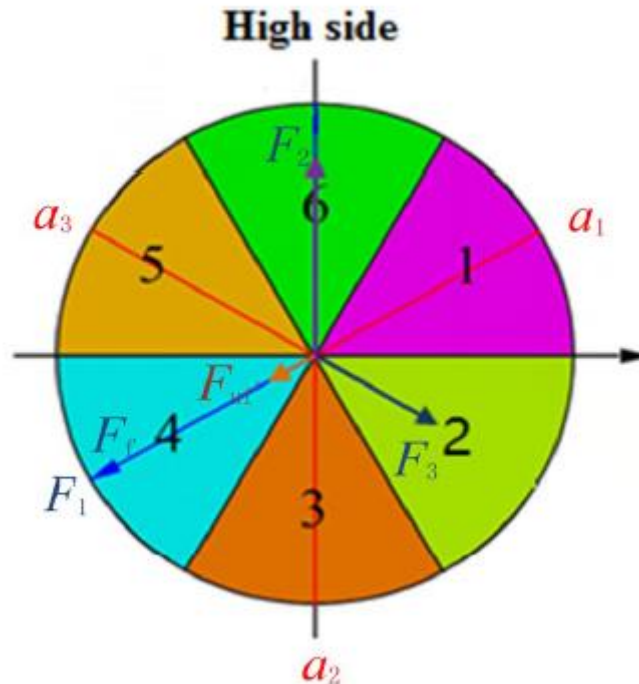
Figure 29: **Six areas of favorability based on the angle between the directions of each wing force and the required steering force**

7.4 Drilling Performance Optimizations

One objective of the competition states that the hole should be drilled as fast as possible by the autonomous drilling rig. In other words, the rate of penetration (ROP) should be as high as possible. To achieve a high ROP, it is planned to use an algorithm that optimizes the mechanical specific energy (MSE) of the drilling process. Alternatively, a machine learning approach will be followed and implemented if time is on hands.

7.4.1 Mechanical Specific Energy

The mechanical specific energy describes the amount of energy required to remove a certain volume of material during a drilling operation. The best efficiency of drilling (high ROP) is given when the minimum mechanical specific energy is reached.

$$MSE = \frac{Total\ Energy\ Input}{Volume\ Removed} \qquad (69)$$

Volume of a drill hole is simply cross-sectional area multiplied by depth of penetration (Δh), and Work Energy can be described as Force multiplied by distance. In drilling there are two forces acting on the bit: Weight on Bit (axial

force) and Torque (rotational force). These are additive to MSE, so there are two terms in the MSE Equation.

$$MSE = \frac{Vertical\ Energy\ Input}{Volume\ Removed} + \frac{Rotational\ Energy\ Input}{Volume\ Removed} \qquad (70)$$

$$MSE = \frac{WOB * \Delta h}{Area * \Delta h} + \frac{Torque * 2\pi * XXX\ of\ Rotations}{Area * \Delta h} \qquad (71)$$

The distance travelled by the bit (Δh) during a given interval is the penetration per time (ROP) divided by rotations per time. This is also known as depth of cut or as Penetration per Revolution.

$$\Delta h = \frac{Penetration\ Per\ Minute}{Rounds\ Per\ Minute} + \frac{ROP}{RPM} = P \qquad (72)$$

This results in

$$MSE = \frac{WOB * \Delta h}{Area * \Delta h} + \frac{2\pi * RPM * Torque}{Area * ROP} \qquad (73)$$

In this equation the MSE is a function of the WOB, the torque and the Penetration per Revolution. In order to find the minimum of the MSE, the equation is only set in dependence of one variable, the WOB. Therefore, the Torque and the Penetration per Revolution must be expressed as function of the WOB. This is possible with two assumptions.

The higher the axial force, the higher the penetration rate and the torsional force. Therefore, the MSE is only displayed as a function of the axial force, i.e. the WOB.

WOB and torque have a linear relationship.

With these assumptions, the penetration per revolution can be described as a quadratic function of the WOB.

$$Torque = f(WOB) = A_0 + A_1 * WOB \qquad (74)$$

$$P = g(WOB) = B_2 * WOB^2 + B_1 * WOB + B_0 \qquad (75)$$

$$P = \frac{ROP}{RPM} \qquad (67)$$

$$MSE = \frac{WOB * \Delta h}{Area * \Delta h} + \frac{2\pi * Torque}{Area * P} \qquad (76)$$

The parameters A_0, A_1, B_0, B_1, B_2 are determined by making test bores in which the WOB, the torque and the penetration per revolution are measured. The insertion in the function of the MSE results in the following equation.

$$MSE = \frac{WOB}{Area} + \frac{2\pi * f(WOB)}{Area * g(WOB)} = \frac{WOB}{Area} + \frac{2\pi * (A_0 + A_1 * WOB)}{Area * B * WOB^2 + B_1 * WOB + B_0} \quad (77)$$

If **Equation 82** is differentiated and set to zero, the optimum torque and penetration per minute can be determined. There are different solutions. The

7.4.2 Machine Learning Approach

With the help of machine learning it is possible to set up and train an algorithm which uses complex statistics to predict a desired value. The basis of any machine learning algorithm is always the availability of a large data set, needed to train the algorithm. On this dataset the algorithm learns the specific relationships between the different values and how they influence the outcome. The greater the dataset and the more diverse, the better the algorithm will get. Ideally, the algorithm can, after being trained, predict the correct outcome from data it has never seen before.

In the scope of the drilling optimization process, it is desired to increase the ROP by influencing the drilling parameters WOB, RPM and pump rate. To determine the best combination of set points for these values a machine learning algorithm could be used. If the mechanical set up of the rig and BHA is finished in adequate time before the competition, a drilling data set could be created by drilling a sandstone sample with a variety of different combinations of drilling parameters for different hole inclinations. For each combination the ROP is measured and added to the data set. A machine learning algorithm, e.g. a Random Forest regressor, could then be set up and be trained on the dataset. Implemented on the rig the algorithm would predict the ideal drilling parameters for a high ROP and provide the system with the values to be used for these parameters.

7.5 Data Visualization

Monitoring the data during the drilling process is crucial for accurate and smooth operations. Data that will be monitored for example to observe the heading of the system. This can be done by plotting the values of the accelerometer and the sensor fusion data. With these datasets the current path of the system can be observed by the user. This is especially important for the testing phase of the system since the actual path of the well can be compared with the desired path and will most certainly be helpful to improve the trajectory control-algorithm. Other values that will be displayed are vibrations and stress of the drill string. These are vital for secure operations of the system since surpassing certain thresholds can be a safety hazard for the system or the user.

The classic drilling parameters, like ROP, WOB, RPM, standpipe pressure, torque and flowrate will also be visualized on a display in a typical manner. These parameters will be displayed in a graphic user interface that is like the ones on large scale rigs. The team will monitor these parameters to make sure everything is going as planned. In that way it is ensured that even if the rig works fully autonomous, the current condition of the drilling operation can always be observed and monitored.

7.6 End of Well Report

Basic information like geological data will be manually entered into the drilling rig. Further, all positional data and drilling data will be saved iteratively every three seconds with a time stamp in a text file. Based on this information, an end of well report will be automatically created after the drilling process is over.

The report will be divided into these categories: Operations summary, geologic summary, well data summary, wellbore schematic, time vs. depth graph, drilling program, mud program and directional program. In the operation summary, the different activities that were performed will be stated, an overview of starting and ending times, drilled and measured depth, kickoff point, build up ratio and an overview over the NPT. The geologic summary will describe the rock that was drilled and its dimensions. The well summary data will show parameters such as RPM, WOB, pump rate, torque, measured depth, true vertical depth, and standpipe pressure. This data will be collected and transferred into an excel file to be attached to the end of well report.

The wellbore schematic will show the trajectory that was taken during drilling and the different coordinate points given. A Time vs Depth graph will show how much time was taken to get to each depth, all activities will be recorded in this time frame. The drilling program will explain in detail the drilling plan. The mud program will state the mud that is used to drill the rock with its rheological values. The directional program will show the different data collected by the BHA sensors near the bit that affect the trajectory. The NPT/Incident report will describe in full detail any problematic shown during the drilling procedure that caused the operation to be delayed or come to a stop.

This report will be used at the end of the competition to create a lesson learned and make a team review of what it was done, what worked and what needs to be improved.

7.7 Third-Party Interface

If the user chooses to steer the drill system remotely, we plan to implement a manual interface where the direction of the drill bit, RPM and WOB can be specified by the user. This can be simply done by ignoring the trajectory control- and optimization-algorithm of the WOB and sending the commands directly over the CAN-bus towards the specified actuators. If enough time is at hand an implementation of an additional joystick for intuitive steering will be investigated.

8 Further Rig Considerations

8.1 Power Consumption

The following values were recorded for the electronics of the entire drilling machine:

Table 4: **Overview power consumption**

Device	Performance [kW]	Performance [HP]
Hydraulic Pump	1.6	2.16
Hoisting Motor	0.18	0.243
Rotary Table Motor	0.18	0.243
Top Drive	1	1.35
Low Hydraulics	0.5	0.675
Remaining Electronics	0.1	0.135
Total	**3.56**	**4.806**

The drilling machine thereby consumes less than one fifth of the maximally allowed 25 horsepower of electrical power.

8.2 Rig Handling

To be able to transport the rig in a practical way, the hoisting traverse is designed to be removable. All electric and hydraulic supply lines are fitted with quick release couplings to reduce preparation time and to prevent the setting of incorrect connections. Once the hoisting traverse is removed it can be mounted horizontally on the supporting rig structure for transportation. In that manner the rig's dimensions are 1600 mm (63 inch) in height, 2050 mm (80.7 inch) in length and 950 mm (37.4 inch) in width. The overall weight of the rig is 250 Kg (551 lbs.) and the chargeable weight 500 Kg (1102 lbs.).

8.3 Funding Plan and Price List

As in previous years, the TU Clausthal Drillbotics® 2021 team is kindly sponsored again from Wintershall Dea, Europe's leading independent gas and oil company. Wintershall Dea will provide the team a total sum of 4000 €. As most of the construction and manufacturing of the different parts of the rig can be done at facilities of the Clausthal University of Technologies, the budget is efficient to buy external mechanical and electronic parts as listed in **Table 5**.

Table 5: Price List

Position	Estimated Price
Materials Rig	
Adjusting unit cylinder	600 €
Motor adjusting unit	125 €
Flex shaft	25 €
Rotary Decoupler	450 €
Cable and Conduits	200 €
Materials BHA	
Hollow shaft	20 €
Bearings	50 €
Steel	150 €
Plastics	100 €
DIN Parts	150 €
Flex shaft	25 €
Steering cylinder	500 €
Drill Bit	
Manufacturing	400 €
Materials	100 €
Rig Electronics	
Stepper Motor	80 €
Stepper Motor Driver	30 €
BHA Electronics	
VFD	120 €
PCB	100 €
BLDC Motor	220 €
Auxiliary Electronics	
STM32	50 €
Accelerometer	55 €
Magnetometer	55 €
Strain Gauges	120 €
Optical Sensor	30 €
Connectors	90 €
Total	**3 835 €**

8.4 Rig Upscaling

Due to the small scale at which the Drillbotics® rig is operated, the opportunity was taken to try out ways of transmitting data, fluids and power that might be foreign to the oil and gas industry. In contrary to real applications in the field we decided do conduct information, hydraulic fluids, and the drilling fluid to the downhole area via cables and hydraulic hoses that are attached to the drill pipe. Since the depth of the borehole is relatively small compared to the diameter of the BHA, this method is applicable. This can be compared to the concept of a wired drill pipe. Here the cables are sealed within the pipe, but the idea of a direct connection is basically the same. But in the end even this technology reaches its limitations, when facing very deep drilling applications with multiple connections.

The torque for the drill bit will be transmitted by a rotating shaft that runs within the drill pipe and is greased to mitigate friction between the surfaces of the two metals. The rotation will be adapted to the needed RPM for the bit by a gearbox seated in the BHA. This might also be considered as very unorthodox. The application of this idea in the field seems not very realistic. The lubricant would not be allowed to flow down the inner annulus and therefore would have to have quite good thixotropic characteristics in the case of downtime. On top of that the additional weight of the rotating shaft would come with additional hook load and stresses inside the drill pipe and shaft would be too high and lead to failure.

Considering the inclination of the BHA in the borehole got inspired by real applications and mirrors the common push-the-bit rotary steerable systems used in many applications. We use wings at the side of the BHA that can be extended according to the desired direction. The difference to the field application lies in the way those wings are controlled. Though they are also moved hydraulically, the hydraulic fluid is pumped from the surface and not integrated into the BHA.

9 Safety Consideration and Risk Analysis

Table 6: Risk analysis

Risk name	Risk description	Risk control strategy
Drilling fluid (water) leaking	Drilling fluid leaks from hose or circulation system	Use suitable hose and circulation system (e.g. hose with appropriate pressure rating capacity). The circulation system will be checked before and while testing.
Pumps working at high pressures	Pumps and hoses were the drilling fluid is flowing through may cause serious damage to personnel and equipment if there is any kind of leaking due to the high pressures	Pumps and valves will be pressure tested before starting any operation, 5 min at low pressure and 10 min at high pressures. At this time only authorized personnel will be allowed to be near the drilling rig. A zone will be set up for visitors or other competitors to not pass through during this time.
String wobbling	String vibration/wobbling	Start drilling at low RPM then increase gradually after reach a certain depth e.g. 1/4". Set the limit of the RPM in algorithm. During this time the string will be observed for any non-normal operations and the vibrations will be recorded to see any abnormalities.
Bit walking	Bit drills deviated away from the trajectory plan. This risk is also associated with string wobbling.	Install a guide shoe or riser/casing at rotary table above the rock sample thus limiting the drill string wobbling. Install downhole sensors, which are accelerometer and gyro, and integrates the acquisition data with algorithm to self-control the drilling trajectory.
Drill string stuck	Drill string stuck due to unclean hole or cutting is not circulated properly from the hole	Apply minimum flow rate according to minimum cutting transport velocity estimation. Apply also minimum drill string rotation speed (RPM) according to design calculation to help hole cleaning.
Loss verticality of hole section	Drill directional hole or deviated trajectory away from the plan	Install downhole sensors (accelerometer and gyro) and integrates acquisition data with algorithm program. Apply algorithm program to maintain verticality to self-control string while drilling.

Drill string buckling and twist off	The weakest part along the drill string is drill pipe. Another potential weak part is connection. Buckling and twist off could occur during the drilling.	Use high strength connection type for all parts of the drill string, particularly the drill pipe. Calculations are made to avoid going over the critical buckling load and set the WOB limit and RPM Estimate the limit strength of drill pipe then limit the WOB and RPM to avoid the failure according to the design calculation. Set the WOB and RPM limit in the algorithm. Avoid going over the critical buckling load. In case much vibration occurs, alert (alarm) system will be active thus students can respond.
Short circuit and/or electrical hazard	The risk is associated with electrical cable or source	Proper handling of electrical cable shall be applied, especially the avoidance from liquid (water). All electrical systems must be set up properly, soldered, installed, and connected to power source carefully and if it is possible enclosed system (use protector) and contained in one place. All the steps associated with setting up electrical must be done with safety concerns and safety protector (if applicable). Minimum safety equipment (e.g. safety glasses, gloves, etc.) must be worn during the electrical installation. No electrical connections should be made when connected to power. Every casing that has electrical components should be grounded to avoid any electrical injury to personnel.
Mechanical construction risk	During build up and/or testing, risk associated with pinch points, punctures, lacerations, cutting debris etc., could cause damage and hazard.	Proper handling of material and pieces during building up the rig structure, particularly it is mandatory to wear the proper HSE equipment according to minimum standard (e.g. safety shoes, safety glasses, gloves, etc.). Students will also work from a certain height during building up the rig structure, thus precautions must be taken to prevent injuries. A certain range of zone isolation must be set thus nonrelated person will be allowed to pass the zone. A general working procedure (Standard Operating Procedure/SOP) will be set before rig construction work. The connection of all parts and pieces

		of rig structure must be checked properly during and after rig construction to confirm the solid rig structure, thus avoiding the loose pieces during the drilling or test. All the sharp edges in rig structure will be covered or protected with protector to avoid human injures. Any items that could potentially fall from any height or loosen through vibrations or high rpm should be secured with a string to some other part, to ensure that no part flies out or falls.
Cutting and drilling fluid spill and disposal	During the drilling, cutting, and drilling fluid will flow out of the well to the surface and must be disposed properly.	Safety containment will be installed around the rock sample and rig structure (below), thus the cutting and drilling fluid circulation (outflow) can be stored properly. The safety containment will be made from transparent material (e.g. plastic, etc.), thus the drilling process can still be observed. Additional storage containment will be installed also to store more cutting and drilling fluid circulation out of the well or rock sample. The cutting and drilling fluid outflow circulation will be recorded and disposed according to regulations (university and state regulations), particularly if there is chemical content. A general procedure will be included together with HSE procedure.
Hazard during drilling or testing	Accident and hazard during drilling or testing could occur.	The drilling automation (through algorithm and computer control) is set up thus less or even no human intervention is needed during the test. However, supervision during the test is still needed. Before the test or drilling is started, safety meeting will be held to discuss the procedure and any potential hazard. Emergency shutdown is included in algorithm program and will active in case serious hazard occurs. The emergency shutdown can also be activated manually (intervention from human) in case the self-control program does not work properly. In case there is obstacle or restriction in circulation system that causing increase of the pressure, emergency shutdown system will be

		activated (included in algorithm) at certain limit of pressure and relief valve is installed to release the pressure. A general testing procedure (Standard Operating Procedure/SOP) will be set before drilling or testing. Minimum HSE equipment standard must be worn (e.g. safety glasses, hearing protection, etc.). A certain range of zone isolation must be set thus unauthorized person will not be allowed to pass the isolation zone. A fire extinguisher will be available on location in case fire occurs due to overheating of electronic components or motor, etc. The hoisting system has locking mechanism to stop the movement in case lost control happens.
Flying debris	Debris that breaks free when cleaning the hole can be unsafe during the drilling process	To maintain the debris confined in the drilling area and to avoid any flying debris to harm anyone around the drilling area, a plastic cover will be installed to protect the personnel around it.
Communication error	Failure during data acquisition due to communication system error	Correct system communications will be controlled by someone in the personnel to ensure good data acquisition and communication between the different systems. System restart will be designed, so whenever data is failed to be acquired, by restarting the system, data acquisition can work properly.
Sensor error	Failure during data acquisition due to sensor failure	The sensors will be tested before and after installation. After each test or drilling, maintenance will be performed to confirm whether the sensors can still function properly.
Mobility of the rig		The mobility of rig is incorporated in the design. The rig structure will be placed above the table and wheels will be installed below the table; thus, the rig can be mobilized. A brake system will be included in wheels to prevent undesired rig movement during drilling or testing due to vibration. Proper handling system will be installed so the rig can be moved safely and in convenient way.

		Modular design will be considered and as far as possible applied in the rig construction, such as electrical, computer, pump and disposal storage that can be disassembled or separated. This will make the mobilization and transportation more convenient and safer.
Rig transport	Pinching of fingers due to handling the rig	To avoid finger pinching the rig will be always handled with a forklift or a portable crane. Wood pieces will be placed on the bottom and sides of the rig when securing it for transportation in case it needs to be handle with the hand to accomplish the correct position. It is prohibited to put a hand under the rig when its being lifted.
Rock sample handling	Personnel can get injured by improperly handling the rock sample	The rock sample will be lifted by a lifting crane, thus avoiding any manual handling from personnel. While lifting the rock sample safety shoes and high impact gloves are to be worn. No other work is to be performed at the time of lifting and unauthorized personnel will be instructed to step back.
Electric cables and water hoses	Cables and hoses lying around which is a serious tripping hazard. Damaging of the equipment, tool failures and health restrictions might be consequences	Cable shafts for electric cables as well as hose guards will be laid to gather the loose components. Additionally, clearly visible warning labels will be put up to make people aware of the hazard

References

Guo, Buyon; Liu, Gefei, 2011. Applied Drilling Circulation Systems; Elsevier Science & Technology

Aadnoy, B. S., 2006. Mechanics of Drilling. Mannheim: Shaker Verlag GmbH.

American Petroleum Institute, 1994. API Bulletin 5C3 - Bulletin on Formulas and Calculations for Casing, Tubing, Drill Pipe, and Line Pipe Properties. 6th ed. Washington DC: s.n.

Bourgoyne Jr., A. T., Millheim, K. K., Chenevert, M. E. & Young Jr., F., 1991. Applied Drilling Engineering. Texas: Society of Petroleum Engineers.

Fairhurst, C. L. W., 1956. Some principles and developments in hard rock drilling techniques. Minnesota Uni., s.n., pp. 15-25.

Han, G; M, Bruno; K, Lao, 2005. Dynamically Modelling Rock Failure in Percussion Drilling. Anchorage, Alaska, ARMA, American Rock Mechanics Association .

Han, G., M, B. & K, L., 2005. Percussion Drilling in Oil Industry: Review and Rock Failure Modelling. Houston, Texas, s.n.

Herbert, G., 1987. Steel Construction Manual. 8 ed. s.l.:American Institute of Steel Construction.

Mitchell, R. F. & Miska, S. Z., 2011. Fundamentals of Drilling Engineering. Richardson, TX: SPE Publishing Services.

Moore, P. L., 1986. Drilling Practices Manual. Texas: PennWell Publishing Company.

Thulin, L., 1971. Mechanics of materials II. s.l.:s.n.

Michaelsen, T., 2018. Lagebestimung durch Sensorfusion mittels Kalmanfilter, Online available at: http://edoc.sub.uni-hamburg.de/haw/volltexte/2018/4392/pdf/Masterarbeit_Tobias_Michaelsen.pdf

Madgwick, S. O. H., 2010. An efficient orientation filter for intertial and intertial/magnetic sensor arrays, Online available at: https://www.x-io.co.uk/res/doc/madgwick_internal_report.pdf

MathWorks®, 2013. Interpolation, Online available at: https://www.mathworks.com/content/dam/mathworks/mathworks-dot-com/moler/interp.pdf

Appendix

A: Drillbotics 2019 Drilling Performance

Unfortunately, the TU Clausthal's drilling rig was not able to drill during the 2019 Drillbotics® competition due to technical failures on the competition's day. Due to the tight time schedule no trial drillings were conducted before the competition took place. Hence, the drilling performance itself can't be discussed as no drilling took place. However, the reasons for the technical failures were investigated and analyzed:

The 2019 team consisted of four students. The workload for the small team was dramatically underestimated which had the consequence that not all functions of the drilling rig could be implemented

Furthermore, relevant functions for the correct operation of the system failed at the day of the competition. This included mainly the electronic components to communicate with the BHA which failed due to short circuits and thermal overload. This routed in a mistake in design as the installed Ic's weren't compatible with the circuit boards. Due to the tight time schedule new, correctly designed circuit boards could not be manufactured before the competition and the problem had to be solved by improvisation. PCB conducting paths were replaced by external conducting paths, which were the main reason for the short circuits as spacing in the BHA became too narrow.

Based on the mistakes from last competition the following conclusions and adjustments were made for this year's design:

- The BHA design was reduced in complexity and sensitive components were shifted to the surface.
- The electrical downhole motor was replaced by a power unit at the surface, which is connected through a flexible shaft to BHA and bit, respectively. Therefore, no control and power electronics, sensitive to failure, are integrated any longer in the BHA. Furthermore, this leads to a saving in space which can be used to install a better steering unit.
- The electrical steering unit of the previous concept will be replaced by a hydraulic steering unit. Power supply and control of the steering unit will be taken over by surface facilities.

B: Data and Assumptions

Based on the 2021 Drillbotics® competition guidelines, some assumptions and basic information for calculation and engineering design are summarized:

Drilling hole and rock data

Drilling hole and rock data	Field unit	Metric unit
Hole diameter (d_h)	1.5 in	38.1 mm
Rock strength	2-5 ksi	13.8-34.5 MPa
Cutting concentration (C_{conc})	1.5%	1.5%
Height of rock	24 in	0.6 m
Cutting density (ρ_s)	165.43 lb/ft^3	2650 Kg/m^3
Diameter cutting (d_s)	0.004 in	0.1 mm
ROP	0.8 ft/hr	0.24 m/hr

Drilling fluid data

Drilling fluid data	Field unit	Metric unit
Water viscosity (μ)	1 cp	0.001 (Pa.s)
Water density (ρw)	8.33 ppg/ 62.428 lb/ft^3	1000 Kg/m^3

Drill pipe data

Steel drill pipe data	Field unit	Metric unit
Ultimate Tensile Strength	73244 psi	505 MPa
Yield strength (Ys)	31183 psi	215 MPa
Modulus of elasticity (E)	2.901x10^7 psi	200 GPa
Weight	0.1493 lb/ft	0.2233 Kg/m
Outside diameter (d_p)	0.393 in	10 mm
Outside radius (r_o)	0.1968 in	5 mm
Inside diameter (id_p)	0.31496 in	8 mm
Inside radius (r_i)	0.15748 in	4 mm
Wall thickness (t)	0.0787 in	2 mm
Length (L_{dp})	36 in	0.91 m
Roughness	0.0006 in	0.0152 mm

Stabilizer/ BHA data

Stabilizer/downhole BHA data	Field unit	Metric unit
Outside diameter (d_d)	1.46 in	37 mm
Diameter Flowline	0.15in	4mm
Length Flowline	0.4 ft	124 mm
Diameter shaft	0.19 in	5 mm
Length shaft	0.19 ft	60 mm
Length (L_{dw})	7.28 in	185 mm
Roughness	0.0039 in	0.1 mm
Inside diameter (id_d)	0.6 in	15.2 mm
Wall thickness (t)	0.1 in	2.54 mm
Length (L_{dw})	3.5 in	8.9 cm
Roughness	0.0006 in	0.0152 mm

Bit data

Bit data [DSATS provided]	Field unit	Metric unit
Bit diameter	1.5 in	38.1 mm
Nozzle diameter	0.118 in	3 mm
Discharge coefficient	0.95	0.95

C: Summary Calculation Results and Formulas

Calculation Results

Parameter	Symbol	Calculated Result	
		Field Units	**Metric Units**
Critical buckling load	P_{bcr}	151.92 lbf	675.77 N
Burst limit	P_{burst}	8326.04 psi	574.06 bar
Torsional Stress limit	τ	218.25 $in.lbf$	24.66 Nm
Flow rate	Q	1.84 gpm	7 Lpm
Pump pressure	P_{pump}	118.76 psi	8.19 Bar
Pump horsepower	HPP	0.12 HP	0.09 kW

Used formulas

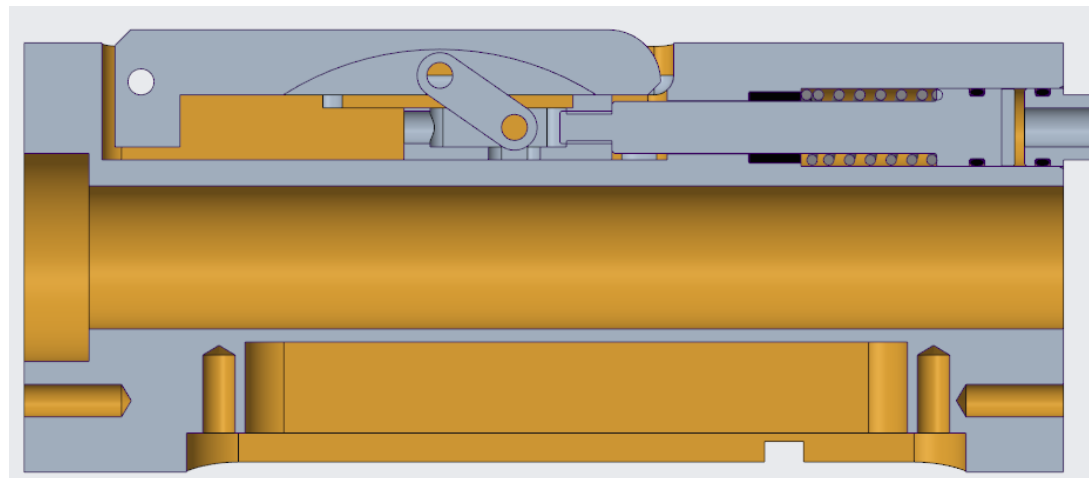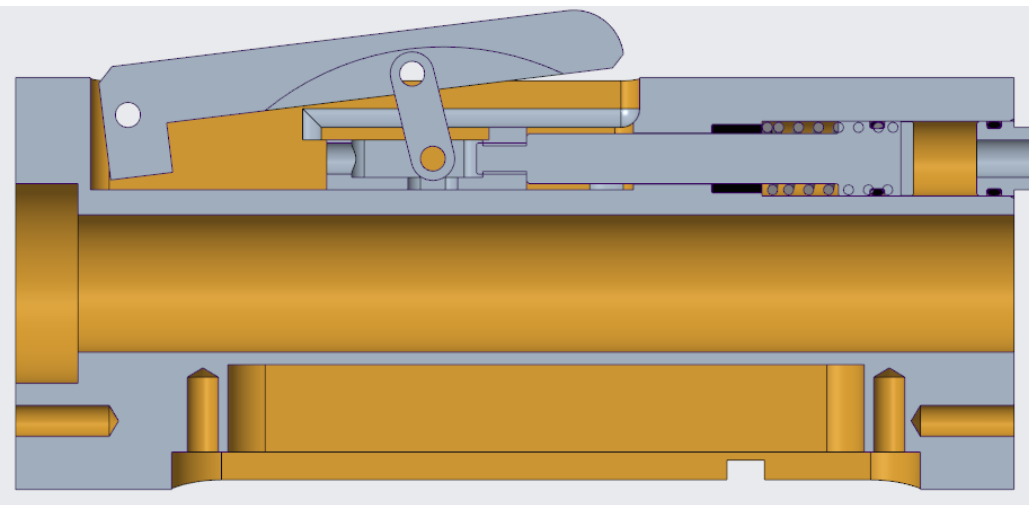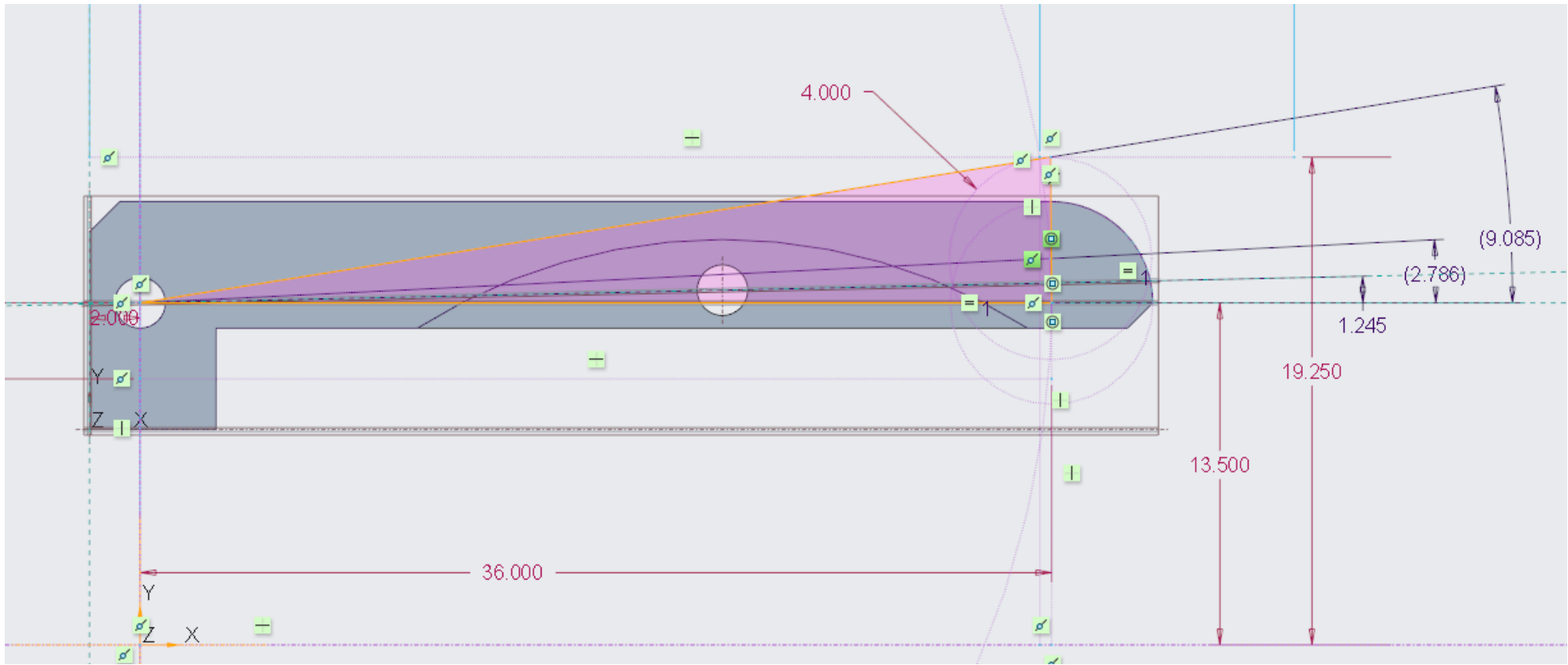| Calculations	Formula	Reference	Results
Reynolds number	$$Re = \frac{928 * \rho_f * v_d * id_p}{\mu_a}$$	Reynolds number (Moore, 1986) (Mitchell & Miska, 2011)	21188 ($Turbulent$)
Friction factor	$$f = 0.25\left[log_{10}\left(\frac{\in}{3.7 * id_p} + \frac{5.74}{Re^{0.9}}\right)\right]^{-2}$$	(Mitchell & Miska, 2011)	0.0301
Pressure loss inside drill pipe	$$P_s = \frac{f * \rho_f * v_d^2 * L_{string}}{25.8 * id_p}$$	(Mitchell & Miska, 2011)	10.48 psi 0.72 bar
Total area of nozzle	$$A_n = 2 * \frac{\pi}{4} * d_n^2$$	Calculation of an area	0.008 in^2 0.053 cm^2
Pressure loss at bit	$$P_{bit} = \frac{Q^2 * \rho_f}{12031 * A_n^2}$$	(Bourgoyne Jr., et al., 1991)	35.06 psi 2.41 bar
Pressure loss in flow line	$$P_{fl} = \frac{f * \rho_f * v_{fl}^2 * L_{fl}}{25.8 * id_{fl}}$$	(Mitchell & Miska, 2011)	42.13 psi 2.9 bar
Pressure loss in shaft	$$P_{sh} = \frac{f * \rho_f * v_{sh}^2 * L_{sh}}{25.8 * id_{sh}}$$	(Mitchell & Miska, 2011)	6.19 psi 0.42 bar
Pressure loss in the BHA	$$P_{BHA} = P_{sh} + P_{fl}$$	(Bourgoyne Jr., et al., 1991)	48.33 psi 3.33 bar

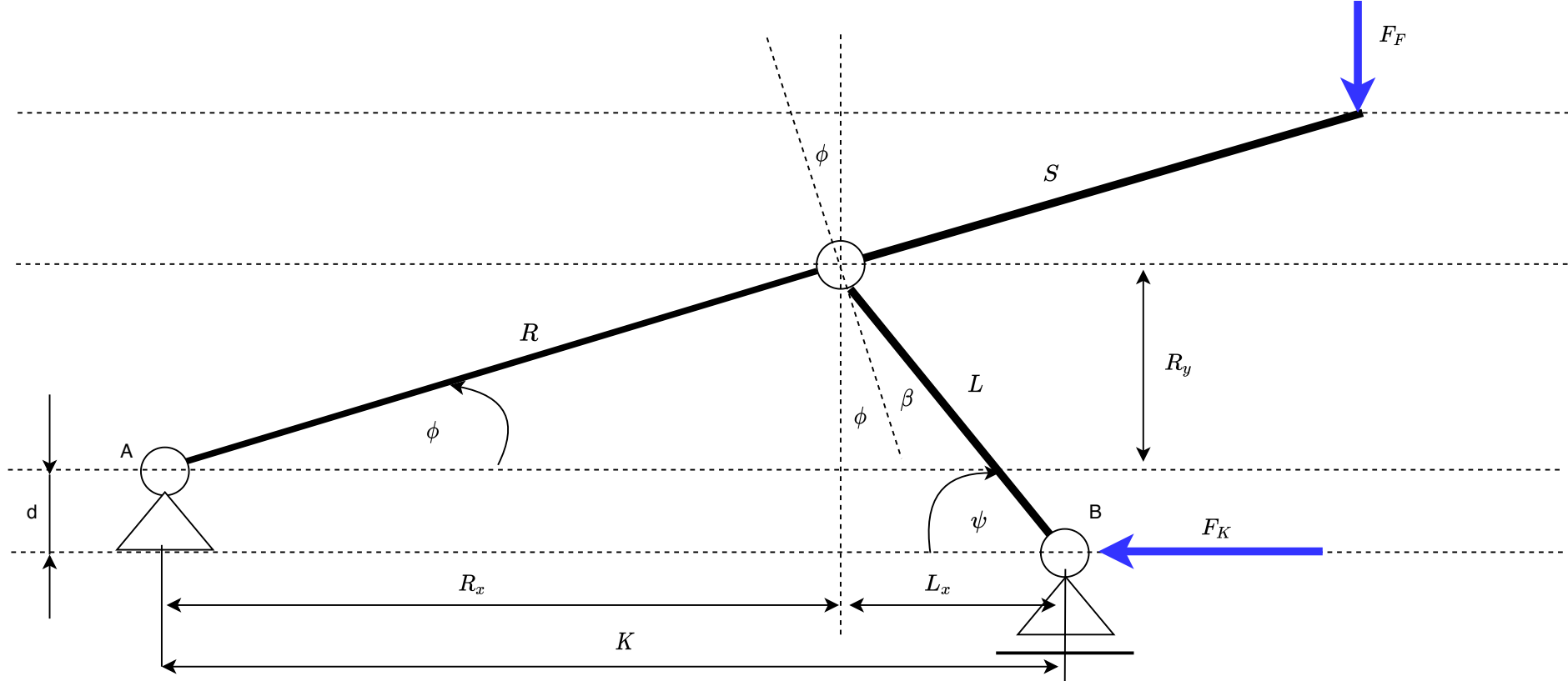|			
Jet impact force	$F_j = 0.01823 * C_d * Q * \sqrt{\rho_f P_{bit}}$	(Bourgoyne Jr., et al., 1991)	$0.54 \, lbf$ $2.43N$
Jet velocity of bit	$v_{bit} = \dfrac{Q}{A_n}$	(Bourgoyne Jr., et al., 1991)	$73.79 \dfrac{ft}{s}$ $22.5 \dfrac{m}{s}$
Pressure loss in annulus	$P_a = \dfrac{1.4327 * 10^{-7} * \rho_f * L_{rock} * v_a^2}{(d_h - d_d)}$	(Bourgoyne Jr., et al., 1991)	$6.8 \, psi$ $0.46 \, bar$
Total downhole pressure loss	$P_{downhole} = P_s + P_{bit} + P_a + P_{BHA}$	(Bourgoyne Jr., et al., 1991)	$100.68 \, psi$ $6.94 \, bar$
Velocity in hose	$v_h = \dfrac{Q}{2.448 * (id_h^2)}$	(Bourgoyne Jr., et al., 1991)	$3.02 \dfrac{ft}{s}$ $0.92 \dfrac{m}{s}$
Reynolds number in hose	$Re = \dfrac{928 * \rho_f * v_h * id_h}{\mu_a}$	Reynolds number (Moore, 1986) (Mitchell & Miska, 2011)	$11678 \, (Turbulent)$
Friction factor determination on Fanning chart	$\dfrac{\epsilon}{id_h}$	Fanning friction factor (Bourgoyne Jr., et al., 1991)	0.0012
Pressure loss inside hose	$P_h = \dfrac{f * \rho_f * v_h^2 * H_{rig}}{25.8 * id_h}$	(Moore, 1986) (Bourgoyne Jr., et al., 1991)	$0.3 \, psi$ $0.02 \, bar$
Total pressure loss along entire system	$P_{loss} = P_{downhole} + P_h$	(Moore, 1986) (Bourgoyne Jr., et al., 1991)	$100.99 \, psi$ $6.96 \, bar$

Total pressure loss with additional atmospheric pressure	$P_{pump} = P_{loss} + P_{atm} + \dfrac{\rho_f * \Delta v^2}{2} + \rho_f * g * \Delta h$	Bernoulli's equation (Mitchell & Miska, 2011)	118.76 psi 8.19 bar
Requirement horsepower for pump	$Pump_{HP} = \dfrac{P * Q}{1714} = \dfrac{352.66 * 3{,}51}{1714}$	(Mitchell & Miska, 2011)	0.12 HP 0.09 kW

D: Control Algorithm Calculations

L_{K0}

R

S

K1

ϕ

U

d

$U_0 = 28,96mm$

$K_0 = 28,75mm$

$\phi_0 = 1,245deg$

R_x

L_x

K_0

$L_{K0} = 36mm$

$R = 23mm$

$L = 7mm$

$d = 3,5mm$

S

K1

R

L

ϕ

U

d

$U_1 = 24,68mm$

$K_1 = R_x + L_x = 24,43mm$

$\phi_1 = 8,245deg$

R_x

L_x

x_K

K_1
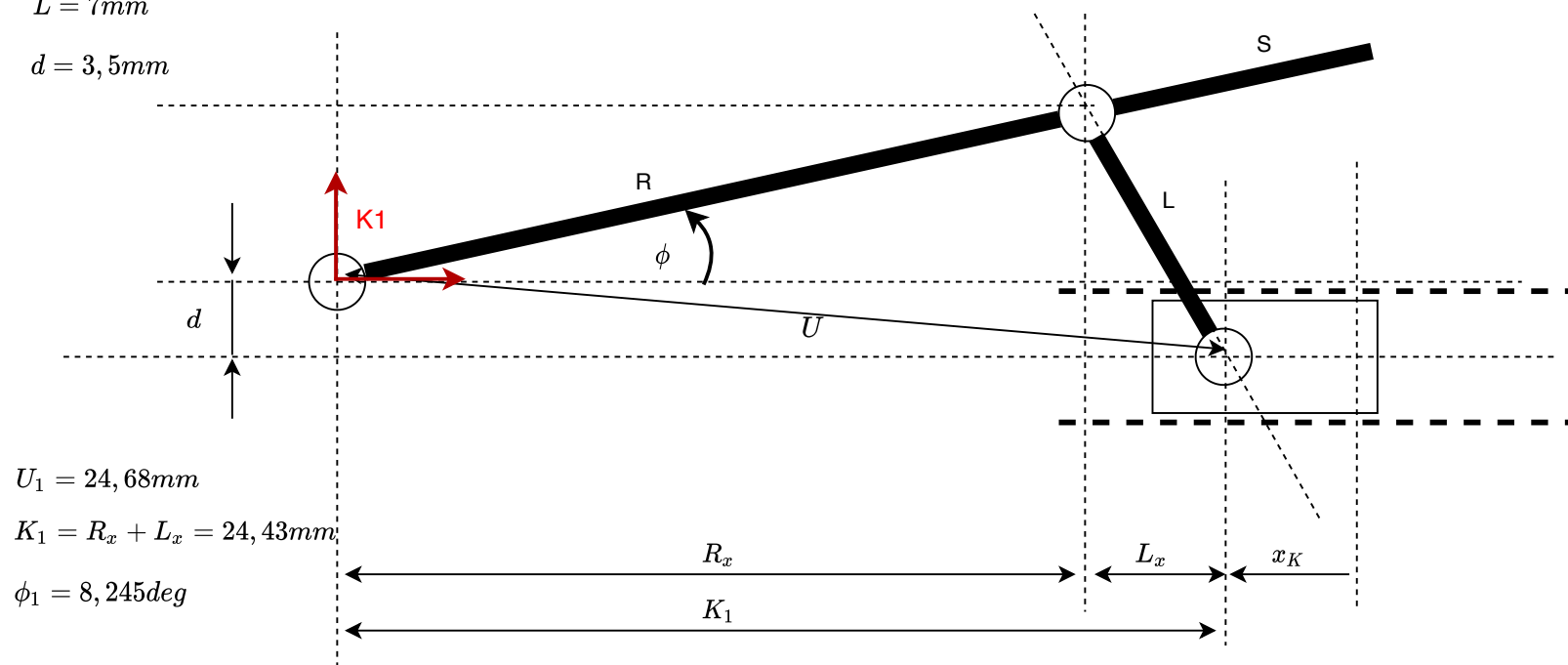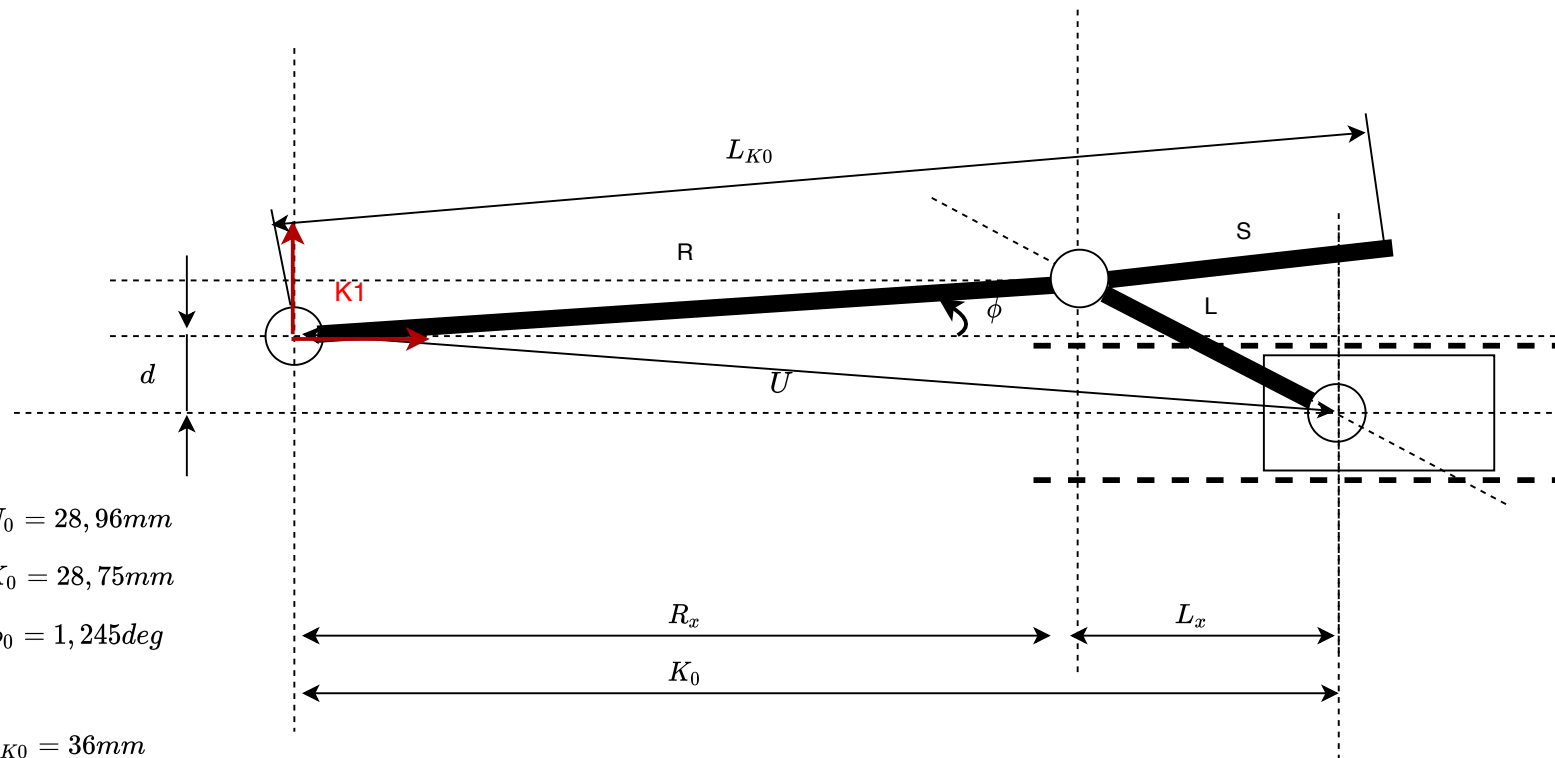
$$K = R \cdot \cos(\phi) + \sqrt{L^2 - (d + R \cdot \sin(\phi))^2}$$

Step 1: Calculate angle β

$$\psi = \sin^{-1}\left(\frac{R_y + d}{L}\right) = \sin^{-1}\left(\frac{R\sin(\phi) + d}{L}\right)$$
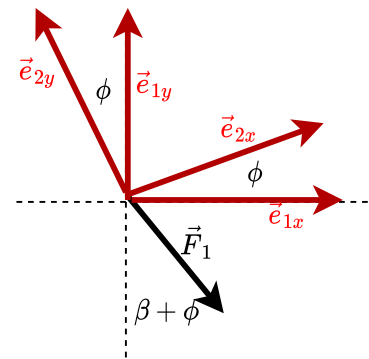
$$\beta = 90° - \phi - \psi$$

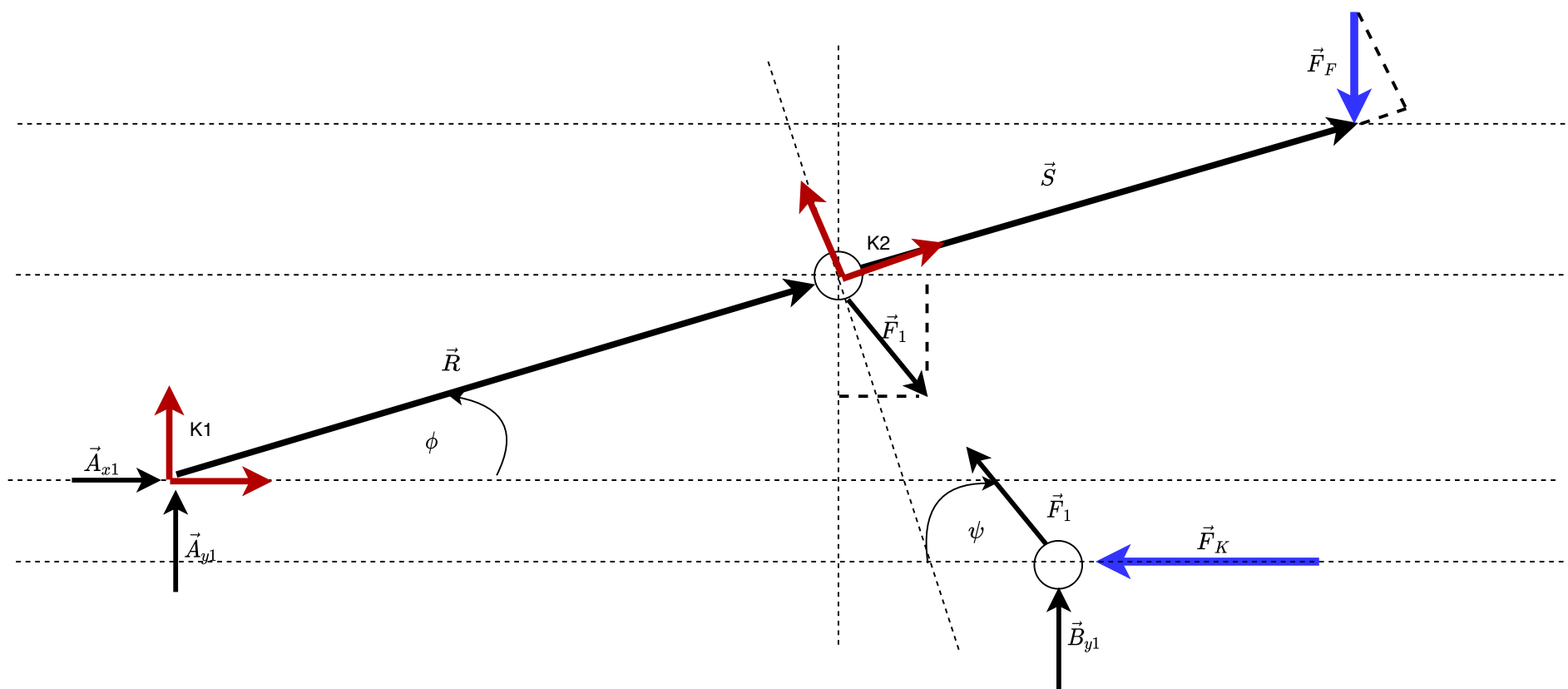Step 2: Transformation from reference frame K1 to K2

$$\vec{e}_{1x} = \cos(\phi) \cdot \vec{e}_{2x} - \sin(\phi) \cdot \vec{e}_{2y}$$

$$\vec{e}_{1y} = \sin(\phi) \cdot \vec{e}_{2x} + \cos(\phi) \cdot \vec{e}_{2y}$$

$$\vec{e}_{2x} = \cos(\phi) \cdot \vec{e}_{1x} + \sin(\phi) \cdot \vec{e}_{1y}$$

$$\vec{e}_{2y} = -\sin(\phi) \cdot \vec{e}_{1x} + \cos(\phi) \cdot \vec{e}_{1y}$$

Step 3: Denote active forces in component notation for reference frame K1 and K2

$$\vec{F}_F = -|\vec{F}_F| \cdot \vec{e}_{1y} = -|\vec{F}_F| \cdot (\sin(\phi) \cdot \vec{e}_{2x} + \cos(\phi) \cdot \vec{e}_{2y})$$

$$\vec{F}_1 = |\vec{F}_1| \cdot \sin(\beta) \cdot \vec{e}_{2x} - |\vec{F}_1| \cdot \cos(\beta) \cdot \vec{e}_{2y} = |\vec{F}_1| \cdot \sin(\beta) \cdot (\cos(\phi) \cdot \vec{e}_{1x} + \sin(\phi) \cdot \vec{e}_{1y}) - |\vec{F}_1| \cdot \cos(\beta) \cdot (-\sin(\phi) \cdot \vec{e}_{1x} + \cos(\phi) \cdot \vec{e}_{1y})$$

Step 4: Define equilibrium of forces for the pads

$$\sum \vec{F} = 0 : \quad \vec{A} + \vec{F}_1 + \vec{F}_F = \vec{0}$$

Step 5: Define equilibrium of torque of the pad around A

$$\sum \vec{M}_A = 0 : \quad \vec{R} \times \vec{F}_1 + \vec{S} \times \vec{F}_F = \vec{0} \qquad |\vec{S}| = L_{K0}$$

Step 6: Define equilibrium of forces for the lever

$$\sum \vec{F} = 0 : \quad \vec{B} + \vec{F}_1 + \vec{F}_K = \vec{0} \qquad \vec{F}_K = -|\vec{F}_K| \cdot \vec{e}_{x1}$$

$$\vec{B} = |\vec{B}| \cdot \vec{e}_{y1}$$

Step 7: Define equilibrium of torque for the lever

$$\sum \vec{M}_B = 0 : \quad \vec{0}$$

Step 7: Define force and position vectors in reference frame K1

$$\vec{A} = \begin{bmatrix} A_{x1} \\ A_{y1} \\ 0 \end{bmatrix}^T \cdot \begin{bmatrix} \vec{e}_{x1} \\ \vec{e}_{y1} \\ \vec{e}_{z1} \end{bmatrix} \qquad\qquad \vec{B} = \begin{bmatrix} 0 \\ B \\ 0 \end{bmatrix}^T \cdot \begin{bmatrix} \vec{e}_{x1} \\ \vec{e}_{y1} \\ \vec{e}_{z1} \end{bmatrix}$$

$$\vec{F}_F = \begin{bmatrix} 0 \\ -F_F \\ 0 \end{bmatrix}^T \cdot \begin{bmatrix} \vec{e}_{x1} \\ \vec{e}_{y1} \\ \vec{e}_{z1} \end{bmatrix} \qquad\qquad \vec{S} = \begin{bmatrix} L_{K0}\cos(\phi) \\ L_{K0}\sin(\phi) \\ 0 \end{bmatrix}^T \cdot \begin{bmatrix} \vec{e}_{x1} \\ \vec{e}_{y1} \\ \vec{e}_{z1} \end{bmatrix}$$

$$\vec{F}_1 = \begin{bmatrix} F_1\sin(\beta+\phi) \\ -F_1\cos(\beta+\phi) \\ 0 \end{bmatrix}^T \cdot \begin{bmatrix} \vec{e}_{x1} \\ \vec{e}_{y1} \\ \vec{e}_{z1} \end{bmatrix} \qquad \vec{R} = \begin{bmatrix} R\cos(\phi) \\ R\sin(\phi) \\ 0 \end{bmatrix}^T \cdot \begin{bmatrix} \vec{e}_{x1} \\ \vec{e}_{y1} \\ \vec{e}_{z1} \end{bmatrix}$$

$$\vec{F}_K = \begin{bmatrix} -F_K \\ 0 \\ 0 \end{bmatrix}^T \cdot \begin{bmatrix} \vec{e}_{x1} \\ \vec{e}_{y1} \\ \vec{e}_{z1} \end{bmatrix}$$

Step 8: Insert force and position vectors in the equilibrium equations

$$\vec{F}_1 = -\vec{A} - \vec{F}_F = -\begin{bmatrix} A_{x1} \\ A_{y1} \\ 0 \end{bmatrix}^T \cdot \begin{bmatrix} \vec{e}_{x1} \\ \vec{e}_{y1} \\ \vec{e}_{z1} \end{bmatrix} - \begin{bmatrix} 0 \\ -F_F \\ 0 \end{bmatrix}^T \cdot \begin{bmatrix} \vec{e}_{x1} \\ \vec{e}_{y1} \\ \vec{e}_{z1} \end{bmatrix}$$

$$\left(\begin{bmatrix} R\cos(\phi) \\ R\sin(\phi) \\ 0 \end{bmatrix}^T \cdot \begin{bmatrix} \vec{e}_{x1} \\ \vec{e}_{y1} \\ \vec{e}_{z1} \end{bmatrix} \right) \times \left(-\begin{bmatrix} A_{x1} \\ A_{y1} \\ 0 \end{bmatrix}^T \cdot \begin{bmatrix} \vec{e}_{x1} \\ \vec{e}_{y1} \\ \vec{e}_{z1} \end{bmatrix} - \begin{bmatrix} 0 \\ -F_F \\ 0 \end{bmatrix}^T \cdot \begin{bmatrix} \vec{e}_{x1} \\ \vec{e}_{y1} \\ \vec{e}_{z1} \end{bmatrix} \right) + \left(\begin{bmatrix} L_{K0}\cos(\phi) \\ L_{K0}\sin(\phi) \\ 0 \end{bmatrix}^T \cdot \begin{bmatrix} \vec{e}_{x1} \\ \vec{e}_{y1} \\ \vec{e}_{z1} \end{bmatrix} \right) \times \left(\begin{bmatrix} 0 \\ -F_F \\ 0 \end{bmatrix}^T \cdot \begin{bmatrix} \vec{e}_{x1} \\ \vec{e}_{y1} \\ \vec{e}_{z1} \end{bmatrix} \right) = \vec{0}$$

$$\vec{F}_K = -\vec{B} - \vec{F}_1 = \begin{bmatrix} -F_K \\ 0 \\ 0 \end{bmatrix}^T \cdot \begin{bmatrix} \vec{e}_{x1} \\ \vec{e}_{y1} \\ \vec{e}_{z1} \end{bmatrix} = -\begin{bmatrix} 0 \\ B \\ 0 \end{bmatrix}^T \cdot \begin{bmatrix} \vec{e}_{x1} \\ \vec{e}_{y1} \\ \vec{e}_{z1} \end{bmatrix} - \left(-\begin{bmatrix} A_{x1} \\ A_{y1} \\ 0 \end{bmatrix}^T \cdot \begin{bmatrix} \vec{e}_{x1} \\ \vec{e}_{y1} \\ \vec{e}_{z1} \end{bmatrix} - \begin{bmatrix} 0 \\ -F_F \\ 0 \end{bmatrix}^T \cdot \begin{bmatrix} \vec{e}_{x1} \\ \vec{e}_{y1} \\ \vec{e}_{z1} \end{bmatrix} \right) = \begin{bmatrix} -A_{x1} \\ -B_{y1} + A_{y1} - F_F \\ 0 \end{bmatrix}^T \cdot \begin{bmatrix} \vec{e}_{x1} \\ \vec{e}_{y1} \\ \vec{e}_{z1} \end{bmatrix}$$

Step 9: Set up systems of equations

$$-\begin{bmatrix} A_{x1} \\ A_{y1} \\ 0 \end{bmatrix}^T \cdot \begin{bmatrix} \vec{e}_{x1} \\ \vec{e}_{y1} \\ \vec{e}_{z1} \end{bmatrix} - \begin{bmatrix} 0 \\ -F_F \\ 0 \end{bmatrix}^T \cdot \begin{bmatrix} \vec{e}_{x1} \\ \vec{e}_{y1} \\ \vec{e}_{z1} \end{bmatrix} - \begin{bmatrix} F_1 \sin(\beta+\phi) \\ -F_1 \cos(\beta+\phi) \\ 0 \end{bmatrix}^T \cdot \begin{bmatrix} \vec{e}_{x1} \\ \vec{e}_{y1} \\ \vec{e}_{z1} \end{bmatrix} = \vec{0} = \begin{bmatrix} -A_{x1} - F_1 \sin(\beta+\phi) \\ -A_{y1} + F_F + F_1 \cos(\beta+\phi) \\ 0 \end{bmatrix}^T \cdot \begin{bmatrix} \vec{e}_{x1} \\ \vec{e}_{y1} \\ \vec{e}_{z1} \end{bmatrix} = \vec{0}$$

$$-\begin{bmatrix} 0 \\ B_{y1} \\ 0 \end{bmatrix}^T \cdot \begin{bmatrix} \vec{e}_{x1} \\ \vec{e}_{y1} \\ \vec{e}_{z1} \end{bmatrix} - \left(-\begin{bmatrix} A_{x1} \\ A_{y1} \\ 0 \end{bmatrix}^T \cdot \begin{bmatrix} \vec{e}_{x1} \\ \vec{e}_{y1} \\ \vec{e}_{z1} \end{bmatrix} - \begin{bmatrix} 0 \\ -F_F \\ 0 \end{bmatrix}^T \cdot \begin{bmatrix} \vec{e}_{x1} \\ \vec{e}_{y1} \\ \vec{e}_{z1} \end{bmatrix} \right) - \begin{bmatrix} -F_K \\ 0 \\ 0 \end{bmatrix}^T \cdot \begin{bmatrix} \vec{e}_{x1} \\ \vec{e}_{y1} \\ \vec{e}_{z1} \end{bmatrix} = \begin{bmatrix} -A_{x1} + F_K \\ -B + A_{y1} - F_F \\ 0 \end{bmatrix}^T \cdot \begin{bmatrix} \vec{e}_{x1} \\ \vec{e}_{y1} \\ \vec{e}_{z1} \end{bmatrix} = \vec{0}$$

$$\begin{bmatrix} 0 \\ 0 \\ F_F R \cos(\phi) - A_{y1} R \cos(\phi) + A_{x1} R \sin(\phi) \end{bmatrix}^T \cdot \begin{bmatrix} \vec{e}_{x1} \\ \vec{e}_{y1} \\ \vec{e}_{z1} \end{bmatrix} + \begin{bmatrix} 0 \\ 0 \\ -F_F L_{K0} \cos(\phi) \end{bmatrix}^T \cdot \begin{bmatrix} \vec{e}_{x1} \\ \vec{e}_{y1} \\ \vec{e}_{z1} \end{bmatrix} = \begin{bmatrix} 0 \\ 0 \\ F_F R \cos(\phi) - A_{y1} R \cos(\phi) + A_{x1} R \sin(\phi) - F_F L_{K0} \cos(\phi) \end{bmatrix}^T \cdot \begin{bmatrix} \vec{e}_{x1} \\ \vec{e}_{y1} \\ \vec{e}_{z1} \end{bmatrix} = \vec{0}$$

$$\begin{bmatrix} -1 & 0 & -\sin(\beta+\phi) & 0 & 0 \\ 0 & -1 & \cos(\beta+\phi) & 0 & 0 \\ -1 & 0 & 0 & 0 & 1 \\ 0 & 1 & 0 & -1 & 0 \\ R\sin(\phi) & -R\cos(\phi) & 0 & 0 & 0 \end{bmatrix} \cdot \begin{bmatrix} A_{x1} \\ A_{y1} \\ F_1 \\ B \\ F_K \end{bmatrix} = \begin{bmatrix} 0 \\ -F_F \\ 0 \\ F_F \\ -F_F(R\cos(\phi) - L_{K0}\cos(\phi)) \end{bmatrix}$$

$$F_1 = \frac{F_F \cdot L_{K0} \cdot \cos(\phi)}{\cos(\beta) \cdot R} \qquad A_{x1} = F_K = -\frac{F_F \cdot L_{K0} \cdot \cos(\phi)}{\cos(\beta) \cdot R} \cdot \sin(\beta+\phi) \qquad A_{y1} = \frac{F_F \cdot L_{K0} \cdot \cos(\phi)}{\cos(\beta) \cdot R} \cdot \cos(\beta+\phi) + F_F \qquad B = \frac{F_F \cdot L_{K0} \cdot \cos(\phi)}{\cos(\beta) \cdot R} \cdot \cos(\beta+\phi)$$

$$\vec{F}_K = \begin{bmatrix} \frac{F_F \cdot L_{K0} \cdot \cos(\phi)}{\cos(\beta) \cdot R} \cdot \sin(\beta+\phi) \\ 0 \\ 0 \end{bmatrix}^T \cdot \begin{bmatrix} \vec{e}_{x1} \\ \vec{e}_{y1} \\ \vec{e}_{z1} \end{bmatrix}$$

$$\psi = \sin^{-1}\left(\frac{R_y + d}{L}\right) = \sin^{-1}\left(\frac{R\sin(\phi) + d}{L}\right)$$

$$\beta = 90° - \phi - \psi$$
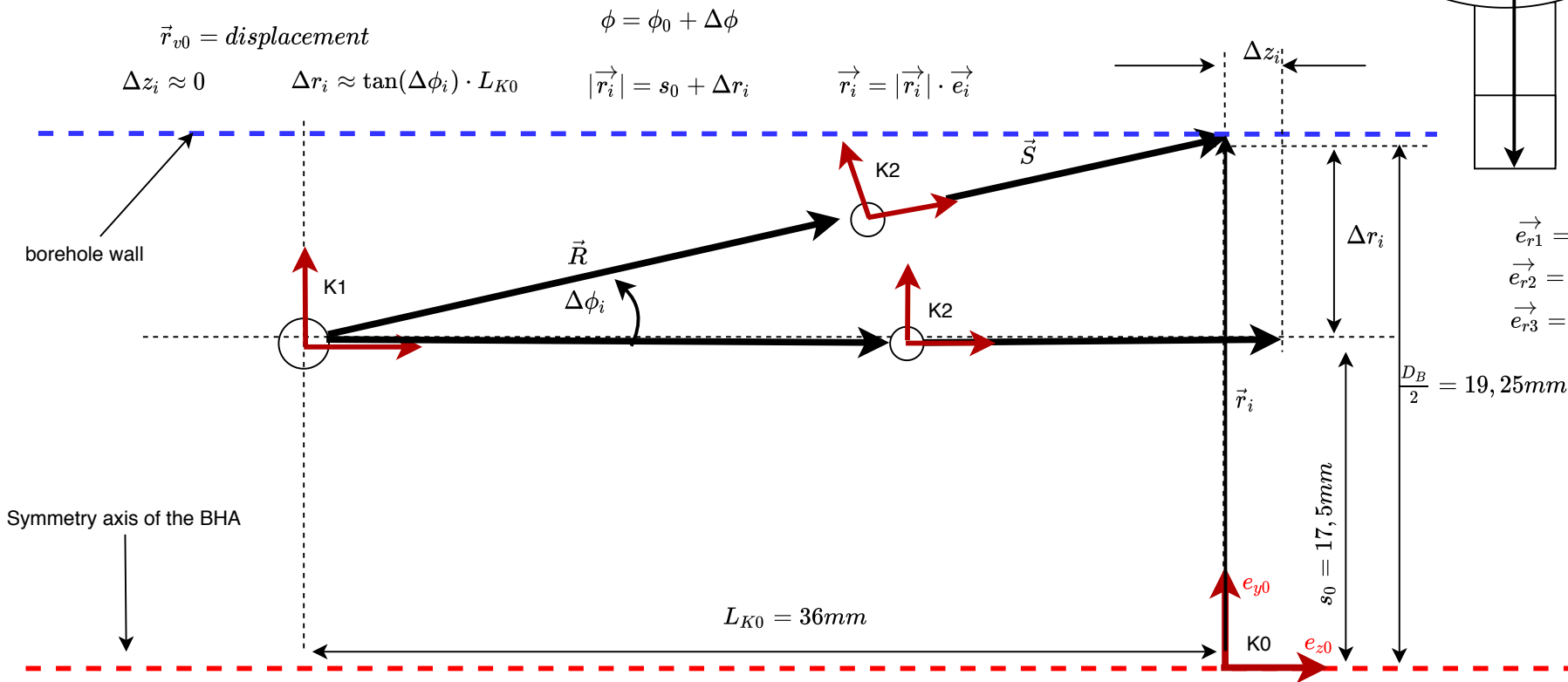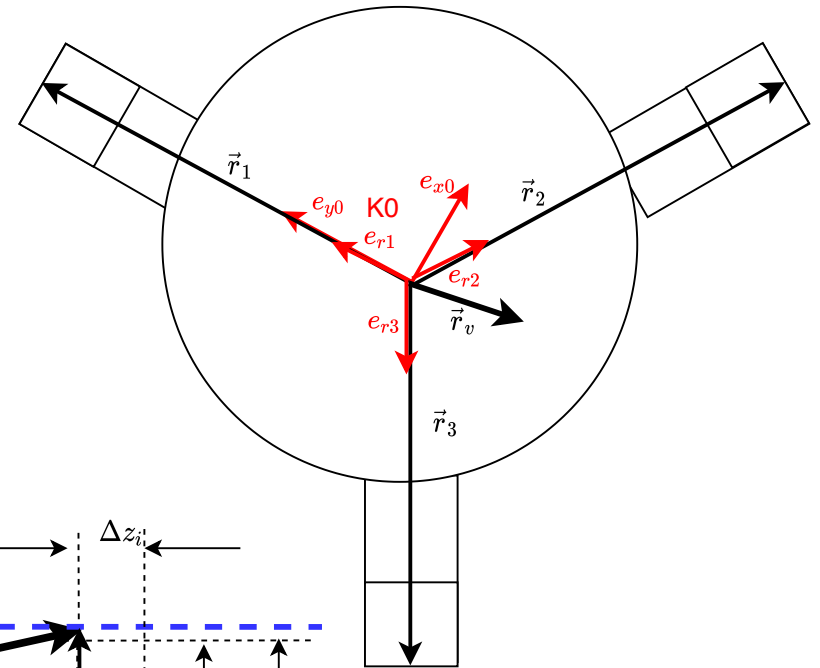
$$\phi = \phi_0 + \Delta\phi$$

Relevant equations

$$x_K = R \cdot \cos(\phi_0 + \Delta\phi) + \sqrt{L^2 - (d + R \cdot \sin(\phi_0 + \Delta\phi))^2} - K_0$$

$$\Delta\phi(x_K) = a_3 x_K^3 + a_2 x_K^2 + a_1 x_K + a_0$$

$\Delta\phi$ must be determined by an interpolation polynomial. The polynomial can be determined from the course of the function x_K.

F_K is the force that must be applied to the piston to apply a defined force F_F to the borehole wall. Thus, the angle correction in the horizontal and vertical planes must be calculated depending on the nominal and actual position of the BHA. The BHA geometry can be used to calculate the displacement vector (location vector at the origin of K0). The direction of the displacement vector is also the direction of the resulting force vector, composed of the three position vectors of the wings. In order to make a change of course now, the individual wing forces must be adjusted so that the resulting force points in the direction of the displacement vector. At the same time, the wings must be adjusted so that no jamming occurs.

$\vec{r}_{v0} = displacement$

$\phi = \phi_0 + \Delta\phi$

$\Delta z_i \approx 0$ $\qquad \Delta r_i \approx \tan(\Delta\phi_i) \cdot L_{K0}$ $\qquad |\vec{r_i}| = s_0 + \Delta r_i$ $\qquad \vec{r_i} = |\vec{r_i}| \cdot \vec{e_i}$

borehole wall

Symmetry axis of the BHA

$L_{K0} = 36mm$

$s_0 = 17,5mm$

$\frac{D_B}{2} = 19,25mm$

$\vec{e_{r1}} = \vec{e_{y0}}$

$\vec{e_{r2}} = \cos(30°)e_{x0} - \sin(30°)\vec{e_{y0}}$

$\vec{e_{r3}} = -\cos(30°)e_{x0} - \sin(30°)\vec{e_{y0}}$

In this case it is assumed in a simplified way that over the entire swivel range $\Delta(z_0)$ is very small. Thus, the position vectors of the wing attack points always lie in the xy-plane.